AMERICAN SOCIETY FOR MICROBIOLOGY | Molecular and Cellular Biology

Negative Regulation of CARD11 Signaling and Lymphoma Cell Survival by the E3 Ubiquitin Ligase RNF181

Sarah M. Pedersen, Waipan Chan,* Rakhi P. Jattani, deMauri S. Mackie, Joel L. Pomerantz

Department of Biological Chemistry and Institute for Cell Engineering, The Johns Hopkins University School of Medicine, Baltimore, Maryland, USA

NF-κB activation downstream of antigen receptor engagement is a highly regulated event required for lymphocyte activation during the adaptive immune response. The pathway is often dysregulated in lymphoma, leading to constitutive NF-κB activity that supports the aberrant proliferation of transformed lymphocytes. To identify novel regulators of antigen receptor signaling to NF-κB, we developed bioluminescence resonance energy transfer-based interaction cloning (BRIC), a screening strategy that can detect protein-protein interactions in live mammalian cells in a high-throughput manner. Using this strategy, we identified the RING finger protein RNF181 as an interactor of CARD11, a key signaling scaffold in the antigen receptor pathway. We present evidence that RNF181 functions as an E3 ubiquitin ligase to inhibit antigen receptor signaling to NF-κB downstream of CARD11. The levels of the obligate signaling protein Bcl10 are reduced by RNF181 even prior to signaling, and Bcl10 can serve as a substrate for RNF181 E3 ligase activity *in vitro*. Furthermore, RNF181 limits the proliferation of human diffuse large B cell lymphoma cells that depend upon aberrant CARD11 signaling to NF-κB for growth and survival in culture. Our results define a new regulatory checkpoint that can modulate the output of CARD11 signaling to NF-κB in both normal and transformed lymphocytes.

The activation of the NF-κB transcription factor downstream of antigen receptor engagement is a critical event required for lymphocyte activation during the adaptive immune response (1, 2). In humans and mice, genetic defects in components of the antigen receptor signaling pathway result in immunodeficiency syndromes in which the failure to mount an effective immune response confers enhanced susceptibilities to infection and impaired clearance of pathogens (3, 4).

CARD11 is a critical signaling scaffold protein that functions to transmit signals from triggered antigen receptors to the IκB kinase (IKK) complex, which inducibly phosphorylates inhibitory IκB proteins, leading to their ubiquitinylation and degradation, which allows NF-κB heterodimers to stably translocate to the nucleus (5–14). During antigen receptor signaling, CARD11 undergoes a transition from a closed, inactive state to an open, active scaffold that recruits several signaling cofactors into a complex that induces IKK kinase activity. CARD11 is kept inactive prior to receptor engagement by an inhibitory domain (ID) that participates in intramolecular interactions that involve the CARD, LATCH, and coiled-coil (CC) domains (15, 16). Triggering of the T cell receptor (TCR) or B cell receptor (BCR) results in the phosphorylation of the ID on specific serines (17–21), which neutralizes its inhibitory activity and allows the signal-induced recruitment of obligate signaling cofactors to CARD11, including Bcl10, MALT1, TRAF6, IKKγ, and caspase-8 (15). The formation and stability of the CARD11-nucleated multiprotein complex dictate the extent and duration of IKK kinase activity and NF-κB activation following antigen recognition, and multiple mechanisms have been described to limit its activity (22). These include the signal-induced degradation of Bcl10 (19, 23–26) and CARD11 (27) and the recruitment of the inhibitory kinesin GAKIN to CARD11, which competes for Bcl10 binding to CARD11 and modulates the CARD11 dwell time at the immunological synapse (28).

It is clear that the failure to appropriately limit or terminate CARD11 signaling can have pathological consequences by contributing to the aberrant growth and survival of transformed lymphocytes. The activated B cell-like (ABC) subtype of diffuse large B cell lymphoma (DLBCL) is characterized by the constitutive, dysregulated activation of NF-κB, which is required for the proliferation of lymphoma cells in culture (29). ABC DLBCL cells require CARD11 for constitutive signaling to NF-κB (30), and ~10% of human ABC DLBCL biopsy specimens display gain-of-function mutations in CARD11 that account for receptor-independent NF-κB activation (31). Lymphoma-associated CARD11 mutations are found in the CARD, LATCH, and coiled-coil domains (31–36) and induce hyperactive CARD11 signaling by disrupting the ability of the ID to keep CARD11 in its closed, inactive state, leading to the spontaneous recruitment of Bcl10 to CARD11 and the subsequent spontaneous activation of the IKK complex and NF-κB (16, 37).

Although it is evident that CARD11 signaling plays a critical role in normal lymphocyte activation and in the dysregulated signaling in ABC DLBCL, the mechanisms that limit the extent of CARD11 signaling in either context are incompletely understood. To identify novel regulators of CARD11 signaling, we developed a novel interaction screening strategy that assays protein-protein interactions in live mammalian cells in a high-throughput manner. Using this strategy, we identified RNF181, a RING finger-containing protein, to be a novel CARD11 interactor. We present

Received 17 September 2015 **Returned for modification** 10 October 2015
Accepted 15 December 2015

Accepted manuscript posted online 28 December 2015

Citation Pedersen SM, Chan W, Jattani RP, Mackie DS, Pomerantz JL. 2016. Negative regulation of CARD11 signaling and lymphoma cell survival by the E3 ubiquitin ligase RNF181. Mol Cell Biol 36:794–808. doi:10.1128/MCB.00876-15.

Address correspondence to Joel L. Pomerantz, joel.pomerantz@jhmi.edu.

* Present address: Waipan Chan, Lymphocyte Biology Section, Laboratory of Systems Biology, National Institute of Allergy and Infectious Diseases, National Institutes of Health, Bethesda, Maryland, USA.

evidence that RNF181 negatively regulates antigen receptor signaling downstream of CARD11 and can influence the signaling output of oncogenic CARD11 variants and the growth of CARD11-dependent human lymphoma cells.

MATERIALS AND METHODS

BRET-based interaction cloning (BRIC). A library of YPet-HA-cDNA fusions was generated by ligating DNA fragments from a normalized human spleen cDNA library (catalog number P12302; Bulldog Bio) into a pcDNA3-derived (Invitrogen) vector carrying YPet (a derivative of yellow fluorescent protein [YFP]) with a C-terminal hemagglutinin (HA) tag. Fragments were size fractionated on an ethidium agarose gel prior to ligation. Clones from this YPet-HA-cDNA library were plated on LB-ampicillin (Amp) agar plates and pooled for minipreparation in pools containing 10 to 70 colonies per pool. Each pool was assayed in a bioluminescence resonance energy transfer (BRET) assay in the presence of CARD11ΔID-Rluc8 as follows.

HEK293T cells were plated at 9×10^4 cells/well in 24-well plates and were transfected 24 h later by the calcium phosphate method with 3 ng of pc-CARD11ΔID-Rluc8 (Rluc8 is a derivative of *Renilla* luciferase) and 60 to 150 ng pool DNA supplemented with pcDNA3 to achieve a total of 350 ng DNA per well. The medium was changed 20 to 24 h later, and at 40 to 44 h after transfection, cells were resuspended in 250 μl 1× Dulbecco's phosphate-buffered saline (DPBS; Gibco) and 90 μl was aliquoted into white 96-well plates (Costar 3912). Coelenterazine-h (catalog number S2011; Promega) was added to the cells to a final concentration of 5 μM, and BRET was measured 10 to 30 min later. The Rluc8 emission was detected over 1 s at 480 nm, and YFP emission was detected over 1 s at 540 nm. For each sample derived from the expression of CARD11ΔID-Rluc8 with a YPet-HA-cDNA library pool, a control sample derived from the expression of CARD11ΔID-Rluc8 alone at the same concentration was assayed in parallel. In addition, CARD11ΔID-Rluc8 was also expressed in the presence of 3 to 30 ng of pcDNA3-YPet and assayed to gauge the levels of bystander BRET of CARD11ΔID-Rluc8 with free YPet.

To calculate milli-BRET (mBRET) values, the background-corrected YPet/Rluc8 ratios of the samples with bait protein alone were subtracted from the YPet/Rluc8 ratios of the samples with the bait protein plus the pool, and the difference was multiplied by a factor of 1,000. Relative YPet acceptor expression was determined independently by measuring YPet fluorescence in black 96-well plates (catalog number 23303; Berthold Technologies) by exciting the cells at 485 nm and recording the emission at 535 nm. The acceptor/donor ratios were calculated by dividing the YPet fluorescence obtained in the acceptor expression assay by the Rluc8 activity obtained in the BRET assay. Measurements were collected using a TriStar LB 941 multimode microplate reader with appropriate excitation and emission filters (Berthold Technologies).

Pools were considered positive in the BRET assay if their calculated mBRET values were at least 3-fold higher than the bystander mBRET values observed with CARD11ΔID-Rluc8 assayed in the presence of free YPet. The cDNA responsible for a positive pool's activity was purified by sib selection and sequenced.

Mammalian expression constructs. CARD11ΔID-Rluc8 was made by cloning a cDNA encoding Rluc8 into pc-CARD11ΔID-FLAG (16) to fuse Rluc8 in frame between CARD11ΔID and the FLAG tag. The full-length human RNF181 cDNA was cloned into pcDNA3 in frame with an N-terminal YPet or FLAG tag, and mutations and truncations were generated in either of these contexts. Expression vectors for CARD11 deletion variants (15, 16) and gain-of-function variants (16, 37) have been described previously.

HEK293T cell reporter assays. HEK293T cells were grown as described previously (15). HEK293T reporter assays were performed using 20 ng of the Igκ$_2$-IFN-LUC NF-κB reporter and 6 ng of the β-galactosidase (β-Gal)-expressing CSK-LacZ control as described previously (15). For Western blotting, lysates with equivalent β-Gal activities in Promega lysis buffer were boiled for 10 min in SDS loading buffer, resolved by SDS-PAGE on 10 or 12% gels, and transferred to polyvinylidene difluoride (PVDF) membranes (catalog number IPVH00010; Millipore). Membranes were blotted with mouse anti-FLAG (catalog number F1804; Sigma), mouse anti-RNF181 (catalog number sc-101120; Santa Cruz), or mouse anti-green fluorescent protein (anti-GFP; catalog number sc-9996; Santa Cruz). The results shown are representative of those from at least three experiments that were performed.

Jurkat T cell reporter assays. Jurkat T cells were grown as described previously (15). Jurkat T cells were plated in 6-well plates at 2.5×10^5 cells per ml and 2 ml/well. The LT-1 transfection reagent (Mirus) was used to transfect cells with 3 μg total DNA following the manufacturer's instructions. Transfections included 200 ng pCSK-LacZ, 1,000 ng Igκ$_2$-IFN-LUC, and the expression vector amounts indicated in the appropriate figure. In each experiment, each sample was supplemented with the empty pcDNA3 expression vector to keep the total amount of transfected DNA constant. At 40 h after transfection, cells were stimulated in 1 ml medium alone or medium supplemented with 1 μg/ml each of mouse anti-human CD3 (catalog number 555329; BD Pharmingen), mouse anti-human CD28 (catalog number 555725; BD Pharmingen), and anti-mouse IgG1 (catalog number 553440; BD Pharmingen) for 4 to 5 h. For tumor necrosis factor alpha (TNF-α) stimulation assays, 75 ng/ml TNF-α (catalog number T6674; Sigma) was used. Nuclear factor of activated T cell (NFAT) assays used 1,500 ng of the NFAT$_4$-IFN-LUC reporter (38) and anti-CD3 in the absence of anti-human CD28 during stimulation. Samples were harvested in 150 μl Promega lysis buffer and assayed for luciferase and β-Gal activity as previously described (15). The results shown are representative of those from at least two experiments that were performed.

Lentivirus-mediated stable knockdown lines. pLKO.1-based lentiviruses expressing short hairpin RNA (shRNA) against a nontarget (NT) control (shNT control; sense sequence, 5′-CAACAAGATGAAGAGCACCAA-3′; loop sequence, 5′-CTCGAG-3′; catalog number SHC002; Sigma), two different shRNAs targeting RNF181, shRNF181-2 (sense sequence, 5′-TGGAGCTCGCAAGGTCACTTT-3′; loop sequence, 5′-CTCGAG-3′) and shRNF181-4 (sense sequence, 5′-CCTCTGCGTCTTCCTTATTAA-3′; loop sequence, 5′-CTCGAG-3′), or an shRNA targeting CARD11 (sense sequence, 5′-TGGTCAAGAAGCTGACGATTC-3′; loop sequence, 5′-TTCAAGAGA-3′) were packaged in HEK293T cells, and Jurkat T cells were infected and selected with 0.5 μg/ml puromycin (Sigma) as previously described (16, 28). Knockdown was assayed by Western blotting using mouse anti-RNF181 (catalog number sc-101120; Santa Cruz), rabbit anti-GAPDH (anti-glyceraldehyde-3-phosphate dehydrogenase; catalog number D16H11; Cell Signaling), rabbit anti-CARMA1 (catalog number 3189; ProSci), rabbit anti-Bcl10 (catalog number sc-5611; Santa Cruz), rabbit anti-MALT1 (catalog number 1664-1; Epitomics), rabbit anti-IKKγ (catalog number sc-8330; Santa Cruz), goat anti-IKKβ (catalog number sc-7329; Santa Cruz), mouse anti-IKKα (catalog number sc-7606; Santa Cruz), rabbit anti-p-IKKα/β (catalog number 2681S; Cell Signaling), and rabbit anti-p65 (catalog number sc-372; Santa Cruz). The results shown are representative of those from at least three experiments that were performed.

HEK293T cell immunoprecipitations. HEK293T cells were transfected by the calcium phosphate method with 2,000 ng total DNA, including 1,500 ng pEBB, 50 to 200 ng of the RNF181 expression construct, 100 to 250 ng of the CARD11 variant expression construct, and the pcDNA3 parental vector. At approximately 40 h after transfection, cells were harvested in 500 μl immunoprecipitation (IP) lysis buffer (15) and incubated for 10 min on ice, and debris was removed by centrifugation at 18,300 × *g* for 10 min at 4°C. The lysates were then precleared by incubating with protein G-Sepharose (bed volume, 7 μl; Amersham) for 30 min at 4°C with rotation. A 4% aliquot was removed for analysis of the IP input. The remaining lysate was incubated with 1 to 2 μg rabbit anti-GFP antibody (catalog number A11122; Life Technologies) for 1 to 1.5 h at 4°C with rotation. Protein G-Sepharose (bed volume, 7 μl) was added to the samples, and the mixtures were incubated for 1 h at 4°C with rotation. The beads were then washed 4 times for 5 min each time at 4°C with IP lysis

buffer before being boiled in the presence of SDS loading buffer. The IPs were analyzed by Western blotting with mouse anti-FLAG (catalog number F1804; Sigma), rabbit anti-GFP (catalog number A11122; Life Technologies), and mouse anti-myc (catalog number sc-40; Santa Cruz). The results shown are representative of those from at least three experiments that were performed.

T cell immunoprecipitations. Jurkat T cells (10^7 cells per sample) were resuspended in RPMI medium alone or with 50 ng/ml phorbol myristate acetate (PMA; Sigma) and 1 μM ionomycin (Sigma) and stimulated for the times indicated in Fig. 1. The cells were then submerged in an ice water bath for 10 min and spun down for 10 min at 423 × *g*. Cell pellets were resuspended in 1.5 ml IP lysis buffer and incubated for 10 min on ice, and the debris was removed by centrifugation at 18,300 × *g* for 10 min at 4°C. Lysates were then precleared twice by incubating with protein G-Sepharose (bed volume, 7 μl; Amersham) for 30 min at 4°C with rotation. A 1.3% aliquot was removed for analysis of the IP input. The lysates were incubated with rotation overnight at 4°C with 2 μg mouse anti-RNF181 (catalog number sc-101120; Santa Cruz) or mouse anti-GFP (catalog number sc-9996; Santa Cruz). Protein G-Sepharose (bed volume, 7 μl) was added to the samples, and the mixture was incubated for 1 h at 4°C with rotation. The beads were then washed 4 times for 5 min each time at 4°C with IP lysis buffer before being boiled in the presence of SDS loading buffer. CARD11 was detected with rabbit anti-CARMA1 (catalog number 3189; ProSci), and RNF181 was detected with mouse anti-RNF181 (catalog number sc-101120; Santa Cruz).

For human $CD4^+$ T cell immunoprecipitations, peripheral blood mononuclear cells were isolated from leukocyte packs (New York Blood Center) via Ficoll gradient separation. $CD4^+$ T cells were then purified to >90% by positive selection with a human $CD4^+$ MultiSort kit (catalog number 130-055-101; Miltenyi Biotec). $CD4^+$ human T cells (6×10^6) were then used for each sample, and immunoprecipitations were performed as described above for Jurkat T cells. The results shown are representative of those from at least two experiments that were performed.

Expression and purification of recombinant proteins in bacteria. Expression vectors for GST-RNF181 and GST-RNF181 R118A were made by cloning the respective RNF181 and RNF181 R118A cDNAs into pGEX6P to fuse the proteins to the C terminus of glutathione *S*-transferase (GST). Proteins were expressed in BL21 bacteria (catalog number 70235-3; EMD Biosciences) as follows. Bacteria were inoculated into 250 ml LB-Amp and grown at 37°C until the optical density at 600 nm (OD_{600}) reached 0.75, and then IPTG (isopropyl-β-D-thiogalactopyranoside) was added to 1 mM to induce protein expression for 3 h. The cultures were cooled in an ice water bath and spun down at 7,700 × *g* for 10 min at 4°C. The pellets were resuspended in 12.5 ml cold phosphate-buffered saline (PBS) containing lysozyme at 0.5 mg/ml, and the mixture was incubated at room temperature for 30 min. The cultures were sonicated 10 times with 5-s pulses at 40% amplitude using a Branson 450 sonifier. Triton X-100 was added to 1%, and the lysates were centrifuged at 10,000 × *g* for 10 min at 4°C. The supernatant was rotated with 400 μl glutathione-Sepharose beads (catalog number 17-5132-01; GE Healthcare) for 1 h at 4°C. The beads were spun down at 500 × *g* for 1 min at 4°C and washed 3 times in 8 ml of 1× PBS (pH 7.4). The beads were then loaded on a column (catalog number 731-1550; Bio-Rad), and bound proteins were eluted in 50 mM Tris HCl, pH 7.5, 10 mM glutathione elution buffer.

To express maltose-bind protein (MBP)–Bcl10, murine Bcl10 cDNA was cloned into pMALC5x to fuse Bcl10 to the C terminus of MBP. MBP-Bcl10 and MBP were expressed in BL21 cells and purified as described above for the GST fusions, except that amylose resin beads (catalog number E80215; NEB) were used, and the proteins were eluted in 50 mM Tris HCl, pH 7.5, 10 mM maltose elution buffer.

To express the myc-tagged CARD–LATCH–coiled-coil (myc-CARD-L-CC) protein, a cDNA encoding these domains was cloned into pET24a(+) in frame with N-terminal V5 and myc tags and a C-terminal 6×His tag. The protein was expressed in Rosetta cells (catalog number 71397-3; EMD Biosciences) as follows. Bacteria were inoculated into 250 ml LB with chloramphenicol and kanamycin and grown with shaking at 30°C until the OD_{600} reached 0.75. IPTG at a final concentration of 1 mM was added to induce expression, and the cells were grown for 2 h at 30°C. The cultures were spun down for 15 min at 6,000 × *g* and 4°C and resuspended in washing buffer (20 mM $Na_2H_2PO_4$, 25 mM NaCl) containing 0.5 mg/ml lysozyme. Samples were freeze-thawed in dry ice, incubated at room temperature for 20 min, and then sonicated 6 times for 5 s each time at 40% amplitude. The cultures were then spun down for 15 min at 6,000 × *g* at 4°C, and a 1-ml bead volume of Talon resin (catalog number 635501; Clontech) was added to the supernatant, followed by rotation at 4°C for 1 h. Samples were spun down at 500 × *g* for 1 min at 4°C and washed 3 times in 10 ml of washing buffer. The beads were loaded on a column and eluted in elution buffer (250 mM imidazole, 500 mM NaCl, 20 mM $Na_2H_2PO_4$).

***In vitro* ubiquitinylation assays.** Ubiquitinylation assays were performed using a ubiquitinylation kit (catalog number BML-UW9920; Enzo Life Sciences) according to the manufacturer's instructions, except that the final total reaction volume was scaled down to 10 μl. The reaction mixtures were placed at 37°C for 1 h, and then 10 μl 2× nonreducing gel loading buffer was added to stop the reaction. The reactions whose results are shown in Fig. 7B used untagged wild-type ubiquitin (Ub; catalog number BML-UW8795-005; Enzo Life Sciences), K48-only ubiquitin (catalog number BML-UW0235-0001; Enzo Life Sciences), or K63-only ubiquitin (catalog number BML-UW0240-0001; Enzo Life Sciences). Samples were boiled, resolved on a 10% SDS-gel, transferred to PVDF membranes, and then analyzed by Western blotting using NeutrAvidin-horseradish peroxidase (HRP) (catalog number 31001; Pierce), mouse anti-RNF181 (catalog number sc-101120; Santa Cruz), rabbit anti-GST (catalog number sc-459; Santa Cruz), mouse anti-MBP (catalog number E8032S; New England BioLabs), rabbit anti-Bcl10 (catalog number sc-5611; Santa Cruz), and anti-myc (catalog number sc-40; Santa Cruz). The results shown are representative of those from at least two experiments that were performed.

GST-S5a (ubiquitin-interacting motif) immunoprecipitation. Jurkat cells (10^7) expressing either shNT or shRNF181-2 shRNA were incubated with 15 μM MG132 (catalog number C2211; Sigma) for 2 h. The cells were then spun down for 10 min at 423 × *g*. The cell pellets were resuspended in 1.5 ml Ub-IP lysis buffer (20 mM Tris, pH 7.5, 150 mM NaCl, 1 mM EDTA, 10% glycerol, 1% Triton X-100, 30 mM NaF, 2 mM Na^+ pyrophosphate) supplemented with 1:1,000 protease inhibitor cocktail (catalog number P8340; Sigma) and 5 mM *N*-ethylmaleimide (NEM; catalog number E3876-5G; Sigma) and incubated for 10 min on ice, and the debris was removed by centrifugation at 18,300 × *g* for 10 min at 4°C. A 1.3% aliquot was removed for analysis of the IP input. The lysates were incubated with rotation for 2 h at 4°C with 10 μg GST-S5a (catalog number I1620; UBPBio). Glutathione-Sepharose (bed volume, 7 μl; Amersham) was added to the samples, and the mixture was incubated for 1.5 h at 4°C with rotation. The beads were then washed 4 times for 5 min each time at 4°C with Ub-IP lysis buffer supplemented with NEM, before being boiled in the presence of SDS loading buffer. Western blot analyses were performed using mouse anti-RNF181 (catalog number sc-101120; Santa Cruz), rabbit anti-Bcl10 (catalog number sc-5611; Santa Cruz), and mouse anti-monoubiquitinylated and anti-polyubiquitinylated conjugates (catalog number BML-PW8810-0100; Enzo Life Sciences). The results shown are representative of those from at least two experiments that were performed.

OCI-Ly3 proliferation and survival assay. OCI-Ly3 cells stably expressing the ecotropic receptor mCAT-1 (16) were cultured in OCI medium, which contains Iscove's modified Dulbecco medium supplemented with 20% human serum (catalog number S40110; Atlanta Biologicals), 50 U/ml each of penicillin and streptomycin, and 55 μM β-mercaptoethanol, in the presence of 2 μg/ml blasticidin in a humidified 5% CO_2 atmosphere at 37°C. These cells were infected with retroviral constructs based on the vector pSUPER.retro.neo+GFP (pSRGN; Oligoengine) and constructed to express either shRNF181-2 (sense sequence, 5′-TGGAGCTC GCAAGGTCACTTT-3′; loop sequence, 5′-CTCGAG-3′), shCARD11-2

(sense sequence, 5′-TGGTCAAGAAGCTGACGATTC-3′; loop sequence, 5′-TTCAAGAGA-3′) (16), or the shNT control (sense sequence, 5′-TTCTCCGAACGTGTCACGT-3′; loop sequence, 5′-TTCAAGAGA-3′) (16) downstream of the H1 RNA promoter and the enhanced green fluorescent protein (EGFP) gene downstream of the phosphoglycerate kinase promoter. Retroviruses were packaged in HEK293T cells as previously described (16). The percentages of GFP-positive (GFP^+) cells were measured on a BD LSR II flow cytometer and analyzed with FlowJo (version 7.6.5) software. The percentage of GFP^+ cells at 3 days postinfection ranged from approximately 5% to 12%. For each infection, the percentages of GFP^+ cells measured throughout the period of culture were normalized to those observed on day 3 postinfection. For Western blot analysis, at day 16 postinfection sihRNF181-2-expressing cells were sorted into GFP-negative (GFP^-) and GFP^+ fractions on a FACSCalibur flow cytometer by the Ross Flow Cytometry Core Facility at The Johns Hopkins University School of Medicine. Two hundred thousand GFP^- and GFP^+ cells were obtained and lysed in IP lysis buffer. Cells were boiled in SDS and resolved on a 12% gel, and Western blotting was performed with mouse anti-RNF181 (catalog number sc-101120; Santa Cruz), rabbit anti-CARMA1 (catalog number 3189; ProSci), rabbit anti-Bcl10 (catalog number sc-5611; Santa Cruz), rabbit anti-GAPDH (catalog number D16H11; Cell Signaling), rabbit anti-IKKγ (catalog number sc-8330; Santa Cruz), goat anti-IKKβ (catalog number sc-7329; Santa Cruz), mouse anti-IKKα (catalog number sc-7606; Santa Cruz), rabbit anti-IκBα (catalog number sc-371; Santa Cruz), mouse anti-phosphorylated IκBα (catalog number 9246S; Cell Signaling), and rabbit anti-p65 (catalog number sc-372; Santa Cruz).

RESULTS

Identification of RNF181 as a CARD11 interactor using BRIC. We developed a novel protein-protein interaction screening strategy that can identify interactions in live mammalian cells. The strategy is based upon bioluminescence resonance energy transfer (BRET), which occurs between appropriate donor and acceptor proteins only when they are positioned in the appropriate orientation within ~100 Å of each other (39). In this approach, which we term BRET-based interaction cloning (BRIC), a bait protein is fused to Rluc8, a derivative of *Renilla* luciferase (40), and screened in mammalian cells in the presence of a prey library consisting of cDNAs fused to YPet, a derivative of YFP (41) (Fig. 1A). Cells are treated with coelenterazine-h, an Rluc8 substrate, and the enzyme-substrate reaction has the potential to generate resonance energy that can excite YPet when transferred in close proximity. A luminometer fitted with appropriate emission filters can quantitatively measure the BRET signal as well as bait protein-Rluc8 activity. For screening, HEK293T cells are transiently transfected with an expression vector for a bait protein-Rluc8 fusion along with pools from an expression library of YPet-cDNA fusions. Pools that yield a positive BRET signal after coelenterazine-h treatment are then deconvoluted by sib selection to identify the individual YPet-cDNA fusion responsible for the BRET signal via its interaction with the bait protein in live cells.

We used this strategy to identify novel CARD11 interactors, using a bait protein of Rluc8 fused to the C terminus of the CARD11ΔID deletion mutant, which is constitutively active due to the absence of the inhibitory domain (ID) that keeps CARD11 in a closed, inactive conformation in the absence of antigen receptor engagement (15, 18). We generated a prey library consisting of YPet fused at the C terminus to cDNAs derived from human spleen and screened cDNA pools of an average complexity of 50 cDNAs per pool for BRET with CARD11ΔID-Rluc8. Pools were considered positive if their calculated mBRET values (see Materials and Methods) were at least 3-fold higher than the bystander mBRET values observed with CARD11ΔID-Rluc8 assayed in the presence of free YPet. One pool, pool C, exhibited the highest BRET signal in the screen. The DNA from pool C was used to retransform bacteria, and individual clones were then evaluated in the BRET assay to identify the clone responsible for the pool's activity (Fig. 1B), which identified clone C3 to be a putative positive CARD11ΔID interactor. Titration of clone C3 in the BRET assay with CARD11ΔID-Rluc8 revealed a strong dose-dependent BRET that was much greater than the background BRET observed with free YPet over the same acceptor/donor range (Fig. 1C). Clone C3 encoded YPet fused to the complete cDNA for human RNF181, a 153-residue RING finger protein that has not been previously implicated in lymphocyte signaling.

To verify that RNF181 can associate with CARD11ΔID, we coexpressed YPet-RNF181 with either wild-type CARD11 or CARD11ΔID in HEK293T cells and immunoprecipitated YPet-RNF181 using anti-GFP antibodies, which recognize YPet. In this assay, YPet-RNF181 interacted with CARD11ΔID but not with wild-type CARD11 (Fig. 1D). The ID prevents the association of CARD11 with multiple proteins in the absence of antigen receptor signaling via intramolecular interactions with CARD and coiled-coil domains but becomes neutralized, in part by phosphorylation, as a result of antigen receptor triggering. Since the ID could influence the RNF181 association with CARD11, we suspected that the endogenous RNF181 and CARD11 proteins would associate in T cells in a signal-dependent manner. To test this, we treated Jurkat T cells with a time course of PMA-ionomycin and immunoprecipitated using anti-RNF181 antibodies. As expected, RNF181 coimmunoprecipitated with CARD11 in a signal-dependent manner (Fig. 1E). This association was not observed in control Jurkat cells in which CARD11 was stably knocked down by lentivirus-mediated RNA interference (RNAi) (cf. the results for shCARD11-expressing cells to those for shNT-expressing cells), nor was it observed with a control anti-GFP antibody (Fig. 1F). We also observed the association of RNF181 and CARD11 in primary human $CD4^+$ T cells only after treatment with PMA-ionomycin (Fig. 1G). The results verified that RNF181 and CARD11 associate at physiological, endogenous levels of expression in a regulated manner and validated the isolation of RNF181 as a CARD11 interactor using the BRIC approach.

RNF181 is an inhibitor of CARD11 and antigen receptor signaling. To test whether RNF181 could modulate CARD11 signaling, we assayed the effect of YPet-RNF181 on the activation of $Ig\kappa_2$-IFN-LUC, an NF-κB reporter, by CARD11ΔID in HEK293T cells. In a dose-dependent manner, YPet-RNF181 inhibited CARD11ΔID-mediated NF-κB activation without diminishing the levels of expression CARD11ΔID (Fig. 2A), suggesting that RNF181 is a CARD11 inhibitor. To assess whether RNF181 functions as an inhibitor at endogenous, physiological levels of expression, we used lentivirus-mediated RNAi to stably knock down RNF181 in Jurkat T cells. Two different shRNAs, shRNF181-2 and shRNF181-4, achieved a >90% knockdown of endogenous RNF181 expression compared to that observed with the shNT control (Fig. 2B). After stimulation with anti-CD3/anti-CD28 antibodies to induce TCR signaling, both shRNF181-2- and shRNF181-4-knockdown cell lines displayed enhanced NF-κB activation compared to that observed with the control shNT-expressing Jurkat cell line, consistent with a role for RNF181 as an

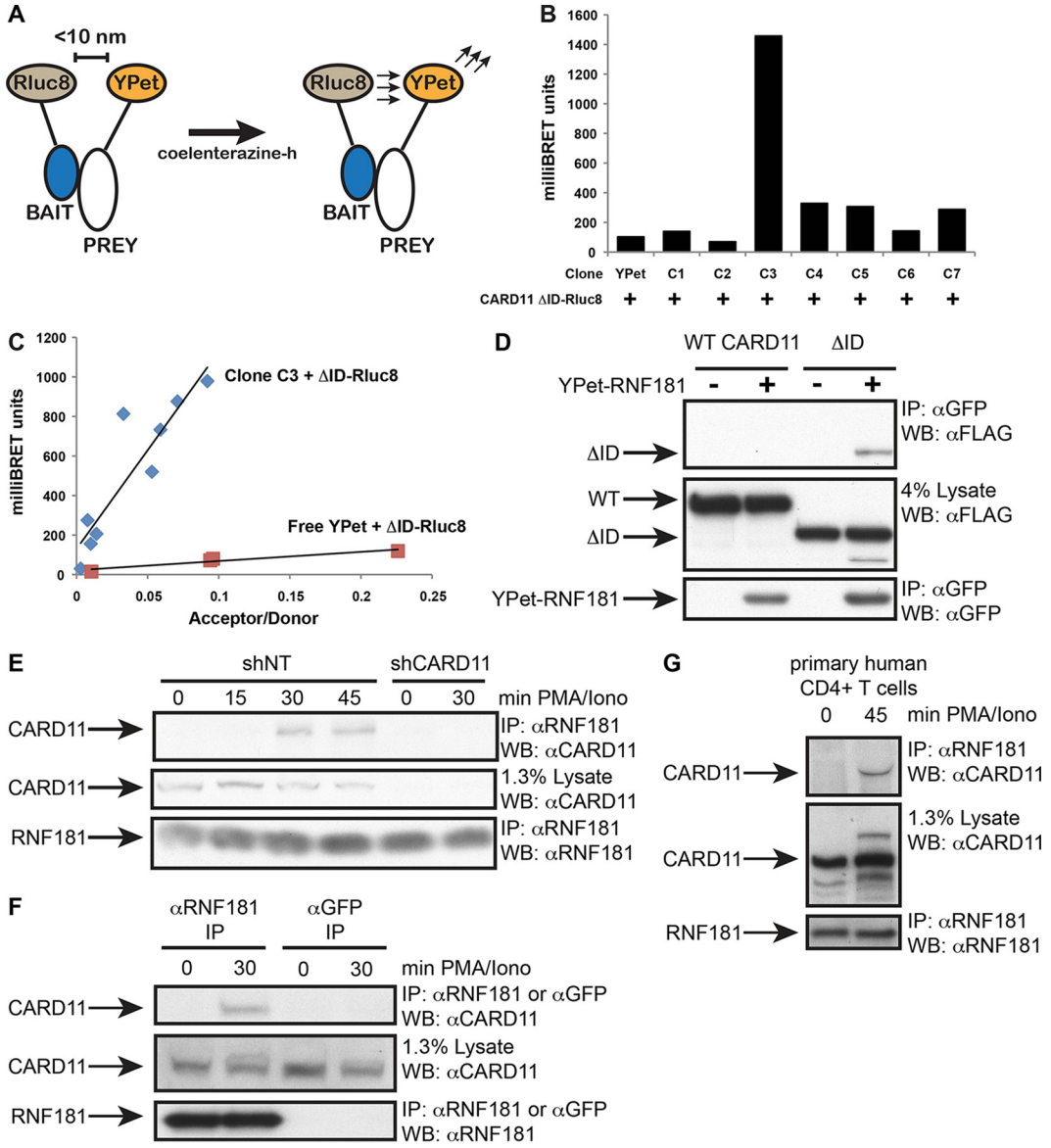

FIG 1 Isolation of RNF181 as a CARD11 interactor in BRET-based interaction cloning. (A) Detection of a protein-protein interaction in live cells by BRET between the appropriate fusions of bait and prey proteins. (B) Clones C1 to C7 from pool C were assayed for BRET in the presence of CARD11ΔID-Rluc8, and the BRET was compared to the bystander BRET observed with free YPet. (C) Clone C3 and free YPet were titrated in the BRET assay in the presence of CARD11ΔID-Rluc8 over a comparable range of acceptor/donor ratios. (D) YPET-RNF181 was coexpressed in HEK293T cells with either FLAG-tagged wild-type (WT) CARD11 or CARD11ΔID (ΔID), and immunoprecipitations were performed using anti-GFP antibodies, as described in Materials and Methods. (E) CARD11-deficient (shCARD11-expressing) or control (shNT-expressing) Jurkat T cells were stimulated with PMA-ionomycin (PMA/Iono), as indicated, and immunoprecipitations using anti-RNF181 antibodies were performed as described in Materials and Methods. (F) shNT-expressing Jurkat T cells were stimulated as indicated, and immunoprecipitations using anti-RNF181 antibodies or anti-GFP control antibodies were performed as described in Materials and Methods. (G) Purified human primary $CD4^+$ T cells were stimulated with PMA-ionomycin, as indicated, and immunoprecipitations using anti-RNF181 antibodies were performed as described in Materials and Methods. WB, Western blotting.

inhibitor of antigen receptor signaling (Fig. 2C). Importantly, the phenotype observed with each of these hairpin RNAs was rescued upon cotransfection of a hairpin RNA-resistant cDNA for RNF181 (RNF181-shr), confirming the specificity of the RNAi effect (Fig. 2C). Furthermore, the knockdown of RNF181 had no effect on the anti-CD3-induced activation of NFAT (Fig. 2D) and no effect on NF-κB activation in response to TNF-α (Fig. 2E). The results indicate that RNF181 is a pathway-specific, transcription factor-specific inhibitor of TCR signaling to NF-κB.

The coiled coil is required for CARD11 association with RNF181. We next used a panel of CARD11 deletion constructs to map the domains of CARD11 required for RNF181 association after coexpression in HEK293T cells (Fig. 3A). As shown in Fig. 3B to D, only the coiled coil was required for RNF181 binding. The involvement of this domain in RNF181 association is consistent with the interaction being regulated by the ID, since the ID interacts with the coiled coil in the basal, inactive state prior to receptor engagement (15). Interestingly, deletion of the L3 or SH3 domain

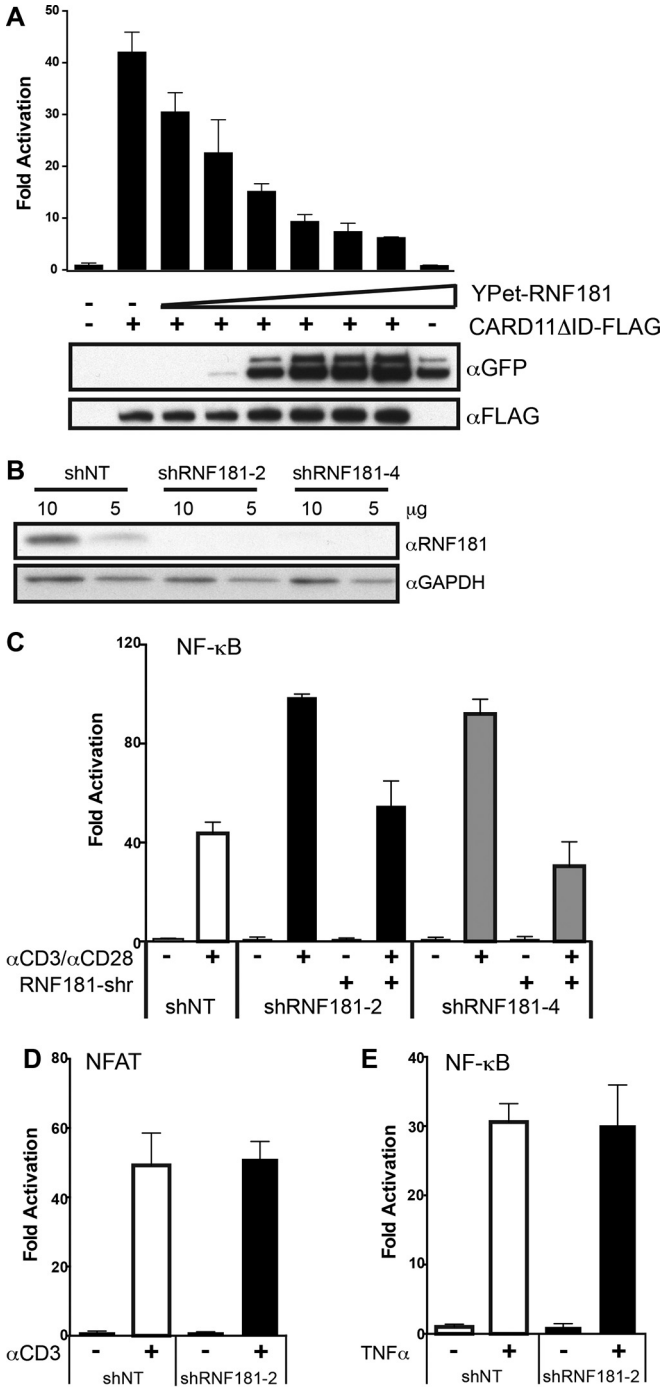

FIG 2 RNF181 is an inhibitor of CARD11 and TCR signaling to NF-κB. (A) HEK293T cells were transfected with Igκ$_2$-IFN-LUC and CSK-LacZ in the presence of CARD11ΔID-FLAG and a titration of YPet-RNF181, as indicated, and assayed for fold activation of the Igκ$_2$-IFN-LUC reporter (top) and expression of YPet-RNF181 and CARD11ΔID-FLAG by Western blotting (bottom). Error bars indicate the standard deviations for 3 samples. A two-tailed unpaired Student *t* test with unequal variance resulted in *P* values of <0.03 for all values obtained in the presence of different doses of YPet-RNF181 compared to the values obtained with CARD11ΔID alone. (B) Jurkat T cells stably expressing the indicated hairpin RNAs were assayed for RNF181 protein expression by Western blot analysis of the indicated amounts of lysate using the indicated antibodies. (C) Jurkat T cells stably expressing the indicated hairpin RNAs were transfected with Igκ$_2$-IFN-LUC and CSK-LacZ in the absence and presence of a hairpin RNA-resistant expression vector for RNF181 (RNF181-shr) and stimulated for 4 h with anti-CD3/anti-CD28, as described in Materials and Methods. Error bars indicate the standard deviations for 3 samples. A two-tailed unpaired Student *t* test with unequal variance resulted in *P* values of <0.003 for the values obtained under stimulated conditions in the presence of either shRNF181-2 or shRNF181-4 compared to the values obtained with shNT. In the presence of a particular hairpin RNA, the same test resulted in *P* values of <0.04 for the values obtained under stimulated conditions with expression of the hairpin RNA-resistant expression vector for RNF181 compared to those obtained without rescue. (D) shRNF181-2- and shNT-expressing Jurkat T cells were transfected with NFAT$_4$-IFN-LUC and CSK-LacZ and stimulated for 4 h with anti-CD3. Error bars indicate the standard deviations for 3 samples. A two-tailed unpaired Student *t* test with unequal variance resulted in a *P* value of 0.89 for values obtained under stimulated conditions with RNF181 knockdown compared to those obtained without knockdown. (E) shRNF181-2- and shNT-expressing Jurkat T cells were transfected with Igκ$_2$-IFN-LUC and CSK-LacZ and stimulated for 4 h with TNF-α. Error bars indicate the standard deviations for 3 samples. A two-tailed unpaired Student *t* test with unequal variance resulted in a *P* value of 0.91 for values obtained under stimulated conditions with RNF181 knockdown compared to those obtained without knockdown.

enhanced RNF181 binding to CARD11 in a statistically significant manner (Fig. 3B to D), suggesting that these domains in the C-terminal half of CARD11 negatively regulate RNF181 binding.

RNF181 is an E3 ubiquitin ligase. The presence of a RING finger in RNF181 suggested that it may function as an E3 ubiquitin ligase. To test this possibility, a GST-RNF181 fusion protein was expressed and purified from bacteria and then incubated in *in vitro* ubiquitinylation reaction mixtures containing biotinylated ubiquitin, recombinant E1, and a panel of E2 enzymes. GST-RNF181 indeed displayed E3 ligase activity *in vitro*, catalyzing the production of polyubiquitin chains, with the highest activity exhibited in the presence of UbcH5a, UbcH5b, UbcH5c, UbcH1, UbcH6, and UbcH13/MMS2 E2 enzymes (Fig. 4A). To obtain a mutant of RNF181 with defective E3 ligase activity, we mutated R118 to alanine, based on the homology of RNF181 to RNF4 and studies that have shown that the homologous arginine (R181) in RNF4 promotes the interaction of the RING finger with both ubiquitin and the E2 during catalysis (42, 43). As shown in Fig. 4B and C, the R118A mutation deleteriously affected the E3 ligase activity of RNF181, as expected, with six different E2 enzymes. In these *in vitro* reactions, we observed polyubiquitin chain production that depended on the addition of E2, on the addition of GST-RNF181, and on the presence of arginine 118. Furthermore, blotting of the reaction mixture with anti-RNF181 antibodies suggested the existence of ubiquitinylated species of RNF181, indicating the possibility that RNF181 can autoubiquitinate in the presence of UbcH5a, UbcH5b, UbcH5c, and UbcH6, at least under these conditions (Fig. 4B and C).

RNF181 E3 ligase activity is required for inhibition of TCR signaling to NF-κB. We next used the R118A mutant of RNF181 to test whether the E3 ligase activity of RNF181 is required for its inhibitory role in antigen receptor signaling. We transiently transfected cells of the RNF181-deficient (shRNF181-2 expressing) Jurkat T cell line with either hairpin RNA-resistant wild-type RNF181 or the R118A mutant and compared their abilities to rescue the phenotype of enhanced anti-CD3/anti-CD28-induced NF-κB activation. While wild-type RNF181 rescued the RNAi phenotype, the R118A mutant failed to do so (Fig. 5A), indicating that R118 and E3 ligase activity are required for inhibition. In this experiment, we used expression vector amounts that achieved comparable levels of expression of wild-type and R118A mutant RNF181 (Fig. 5B).

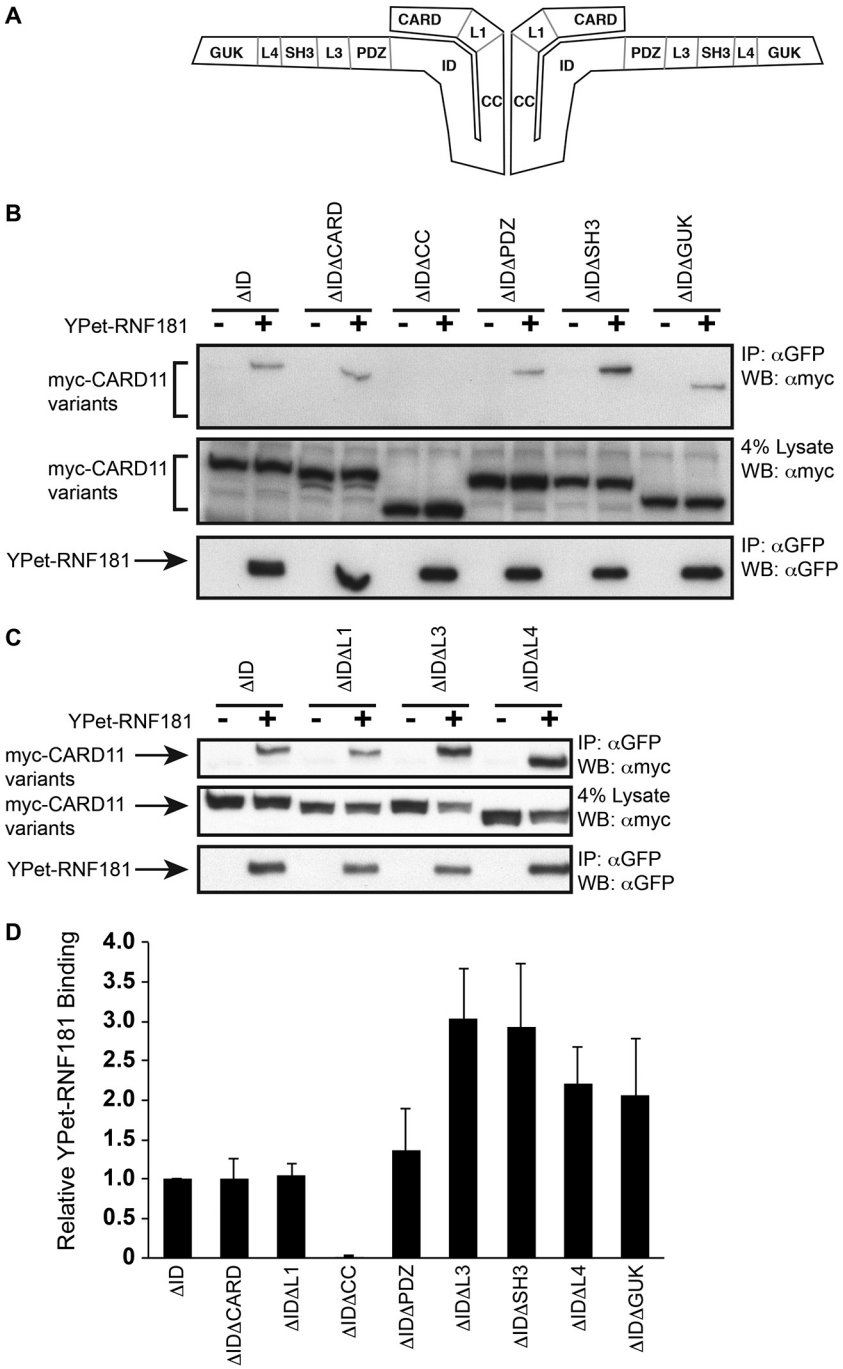

FIG 3 Domain determinants of CARD11 interaction with RNF181. (A) Domain organization of CARD11. The protein is an oligomer but is depicted as a dimer for ease of representation. The LATCH domain resides within the L1 linker. (B and C) HEK293T cells were transfected with expression constructs for YPet-RNF181 and the indicated myc-tagged CARD11 variants, and immunoprecipitations using anti-GFP antibodies were performed as described in Materials and Methods. The results of the experiments shown are representative of those from three repetitions. (D) Quantitation of the relative bound/input ratios of the myc-tagged CARD11 variants pulled down in all experiments, performed as described in for panels B and C. Error bars indicate standard deviations for 3 samples. A two-tailed unpaired Student *t* test with unequal variance resulted in the following *P* values in comparison with the values observed with CARD11ΔID: for ΔIDΔCARD, $P = 0.99$; for ΔIDΔL1, $P = 0.61$; for ΔIDΔCC, $P = 0.000026$; for ΔIDΔPDZ, $P = 0.35$; for ΔIDΔL3, $P = 0.025$; for ΔIDΔSH3, $P = 0.050$; for ΔIDΔL4, $P = 0.068$; for ΔIDΔGUK, $P = 0.12$.

We next wanted to determine whether the RNF181 RING finger domain is sufficient for the inhibitory activity of RNF181 in this pathway. First, we determined that the RING finger is sufficient for the interaction with CARD11ΔID in co-IP experiments using YPet fusions to full-length RNF181 or the RING finger only (Fig. 5C). In addition, the R118A mutation in the context of the YPet-RING fusion had no effect on the ability of the RING finger to associate with CARD11 (Fig. 5C), supporting the notion that

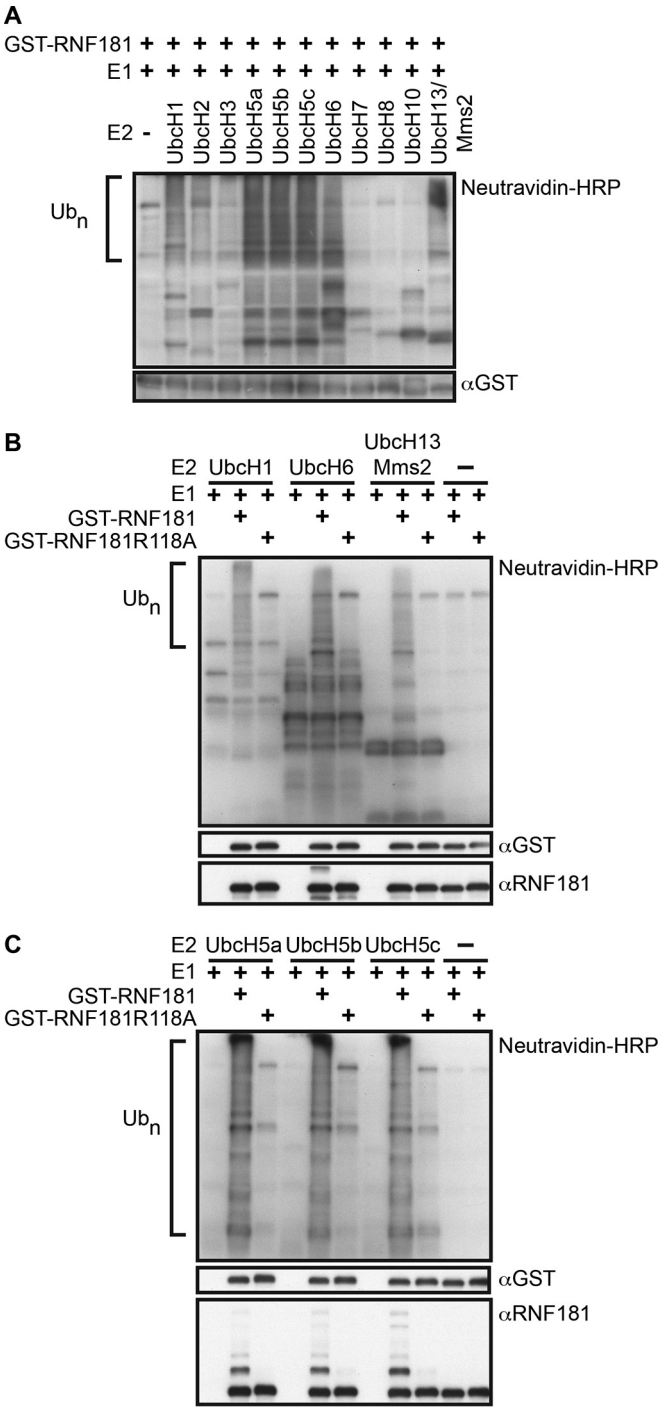

FIG 4 RNF181 is an E3 ubiquitin ligase. (A) Recombinant GST-RNF181 that was expressed in and purified from bacteria was assayed *in vitro* in the presence of biotinylated ubiquitin, E1, and the indicated E2 under ubiquitinylation reaction conditions as described in Materials and Methods. The products of the reaction were resolved and probed with NeutrAvidin-HRP or anti-GST antibodies, as indicated. (B and C) Either recombinant wild-type GST-RNF181 or GST-RNF181 R118A was assayed *in vitro* in the presence of biotinylated ubiquitin, E1, and the indicated E2 under ubiquitinylation reaction conditions, as described in Materials and Methods. The products of the reaction were resolved and probed with NeutrAvidin-HRP, anti-GST or anti-RNF181 antibodies, as indicated.

the R118A mutation does not have inadvertent negative effects on the folding of the RING finger. In the RNAi rescue assay, the RING finger domain was sufficient to rescue inhibitory RNF181 function, while the RING R118A mutant did not rescue the enhanced signaling that resulted from stable RNF181 knockdown (Fig. 5D and E). The results are consistent with the conclusion that the inhibition of CARD11 signaling in the antigen receptor pathway by RNF181 requires its E3 ligase activity. Furthermore, the lack of inhibitory activity of the RING R118A mutant suggests that RNF181 does not inhibit CARD11 solely by associating with CARD11.

Bcl10 levels are elevated in the absence of RNF181. To begin to identify a possible target for RNF181 E3 ligase activity, we treated RNF181-deficient and control Jurkat T cells with a 45-min time course of TCR cross-linking and probed the lysates for the levels of the Bcl10, MALT1, and CARD11 proteins. We found that in RNF181-knockdown cells, Bcl10 levels were reproducibly elevated by 3.2-fold even in the absence of TCR triggering, after normalization to the levels of GAPDH (see the results of a representative experiment in Fig. 6A and B and the quantitation of results from multiple experiments in Fig. 6G). During the 45-min time course of signaling, Bcl10 levels gradually decreased to the level observed in the control shNT-expressing Jurkat T cells. CARD11 levels were also elevated in RNF181-knockdown cells, but to a lesser extent (by 2.4-fold, on average) (Fig. 6A, C, and G). MALT1 levels were not significantly altered by RNF181 depletion (Fig. 6A, D, and G). We also probed RNF181-deficient and control Jurkat T cells for the levels of IKKβ, IKKα, IKKγ, and p65, but the levels of none of these were altered as a result of RNF181 depletion (Fig. 6E and G). Consistent with the inhibitory role of RNF181 on CARD11 signaling, we did observe enhanced levels of TCR-induced phospho-IKKα/β, which is indicative of IKK kinase activation (Fig. 6E to G).

Bcl10 is a substrate for RNF181 E3 ligase activity *in vitro*. Mechanisms that alter Bcl10 protein levels in lymphocytes have previously been shown to influence the output of antigen receptor signaling to NF-κB (19, 23–26). To test whether Bcl10 could serve as a direct substrate for RNF181-mediated ubiquitinylation, we incubated a bacterially expressed MBP-Bcl10 fusion protein with recombinant GST-RNF181 in *in vitro* ubiquitinylation reactions with several E2 enzymes. As shown in Fig. 7A, MBP-Bcl10 was ubiquitinylated by GST-RNF181 in the presence of UbcH5b and UbcH5c but not in the presence of UbcH5a or in the absence of E2, as indicated by the high-molecular-weight species that were reactive with both anti-MBP and anti-Bcl10 antibodies. The MBP control protein was not ubiquitinylated in these reactions, indicating specificity in these reactions for the Bcl10 portion of the MBP-Bcl10 fusion.

We next tested whether RNF181 could ubiquitinylate Bcl10 with K48-linked ubiquitin chains, which would be expected if RNF181 regulated Bcl10 levels by targeting it for proteasomal degradation. As shown in Fig. 7B, GST-RNF181 could ubiquitinylate MBP-Bcl10 with wild-type ubiquitin and with a derivative that can form linkages only through K48 (K48 only) but not with a derivative that can form linkages only through K63 (K63 only).

To probe whether Bcl10 is indeed ubiquitinylated in an RNF181-dependent manner in unstimulated T cells, we isolated K48-linked polyubiquitin-conjugated proteins from MG132-treated RNF181-deficient and control Jurkat T cells via

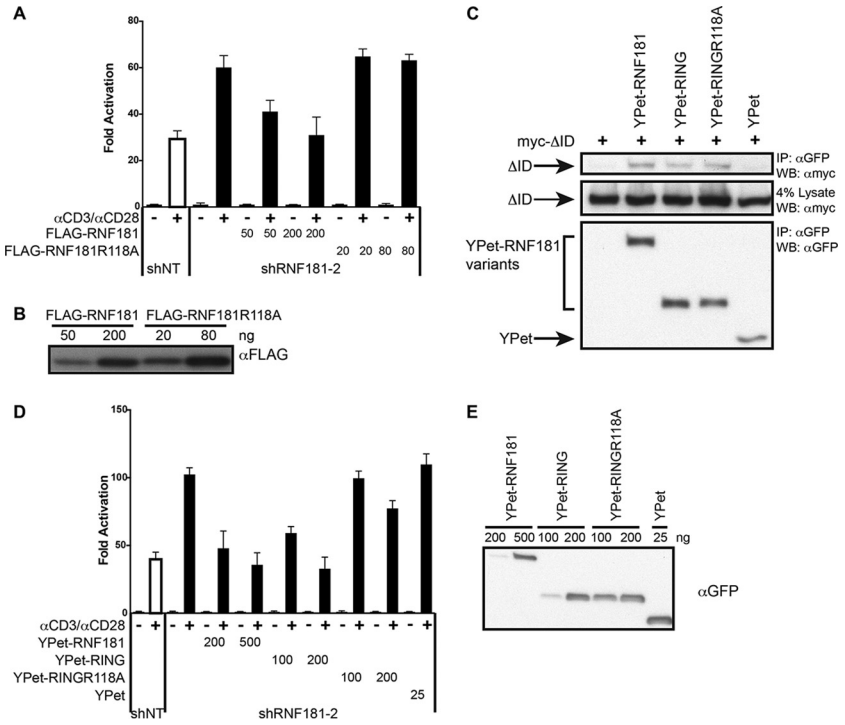

FIG 5 The E3 ubiquitin ligase activity of RNF181 is required for its inhibitory activity. (A) Jurkat T cells stably expressing the indicated hairpin RNAs were transfected with Igκ$_2$-IFN-LUC and CSK-LacZ in the absence and presence of hairpin RNA-resistant expression vectors for FLAG-RNF181 or FLAG-RNF181 R118A and stimulated for 4 h with anti-CD3/anti-CD28, as described in Materials and Methods. Error bars indicate the standard deviations for 3 samples. A two-tailed unpaired Student *t* test with unequal variance resulted in the following *P* values in comparison with the values observed with the shRNF181-2 hairpin RNA without rescue under stimulated conditions: for 50 ng FLAG-RNF181, $P = 0.006$; for 200 ng FLAG-RNF181, $P = 0.01$; for 20 ng FLAG-RNF181 R118A, $P = 0.29$; for 80 ng FLAG-RNF181 R118A, $P = 0.46$. (B) Relative expression levels of FLAG-RNF181 and FLAG-RNF181 R118A after the equivalent amount of vectors used in the assay whose results are presented in panel A were transfected into HEK293T cells. (C) myc-CARD11ΔID was coexpressed in HEK293T cells with the indicated YPet fusions, and immunoprecipitations using anti-GFP antibodies were performed as described in Materials and Methods. (D) Jurkat T cells stably expressing the indicated hairpin RNAs were transfected with Igκ$_2$-IFN-LUC and CSK-LacZ in the absence and presence of hairpin RNA-resistant expression vectors for YPet-RNF181, YPet-RING, YPet-RING R118A, or YPet and stimulated for 4 h with anti-CD3/anti-CD28 as described in Materials and Methods. Error bars indicate the standard deviations for 3 samples. A two-tailed unpaired Student *t* test with unequal variance resulted in the following *P* values in comparison with the values observed with shRNF181-2 hairpin RNA without rescue under stimulated conditions: for 200 ng YPet-RNF181, $P = 0.006$; for 500 ng YPet-RNF181, $P = 0.001$; for 100 ng YPet-RING, $P = 0.0004$; for 200 ng YPet-RING, $P = 0.001$; for 100 ng YPet-RING R118A, $P = 0.54$; for 200 ng YPet-RING R118A, $P = 0.035$; for 25 ng YPet, $P = 0.26$. (E) Relative expression levels of the indicated YPet fusions after the equivalent amount of vectors used in the assay whose results are presented in panel D were transfected into HEK293T cells.

pulldown with a GST-S5a fusion protein and probed the precipitates for the presence of Bcl10. S5a is an integral component of the 26S proteasome that recognizes K48-linked polyubiquitinylated proteins (44). We could detect ubiquitinylated species of Bcl10 in unstimulated control T cells, and lower levels were observed in RNF181-deficient T cells (Fig. 7C), consistent with a model in which RNF181 targets Bcl10 for K48-linked ubiquitinylation.

Since both Bcl10 and RNF181 can interact with CARD11 via the coiled-coil domain, we tested whether the addition of a recombinant CARD–LATCH–coiled-coil (CARD-L-CC) protein representing the N-terminal half of CARD11 would affect the *in vitro* ubiquitinylation of Bcl10 by RNF181. Interestingly, titration of the CARD-L-CC protein into the reaction mixture resulted in the reduced ubiquitinylation of MBP-Bcl10 (Fig. 7D). In these reactions, the CARD-L-CC was itself ubiquitinylated and could serve as a substrate of GST-RNF181 in the presence of UbcH5c and in the absence of MBP-Bcl10 (Fig. 7D, left two lanes). At the same concentrations at which CARD-L-CC inhibited MBP-Bcl10 ubiquitinylation by GST-RNF181, CARD-L-CC had no effect on non-specific GST-RNF181 E3 ligase activity, as indicated by the production of polyubiquitin chains in the reaction (Fig. 7E). The data are consistent with a model in which RNF181 targets Bcl10 for ubiquitinylation prior to the assembly of the CARD11-Bcl10-MALT1 complex and in which Bcl10 recruitment to CARD11 prevents RNF181-mediated conjugation. In addition, the data suggest that the association of RNF181 with CARD11 does not modulate its intrinsic E3 ligase activity.

RNF181 restricts the proliferation of DLBCL cells dependent on hyperactive CARD11 signaling to NF-κB. The activated B cell-like (ABC) subtype of human diffuse large B cell lymphoma (DLBCL) is characterized by the constitutive, dysregulated activation of NF-κB, which is required for proliferation and survival of the lymphoma (29). In ~10% of ABC DLBCL cases, gain-of-function mutations in CARD11 account for the constitutive signaling to NF-κB (31). These DLBCL-associated CARD11 mutations have been found in the CARD, LATCH, and coiled-coil domains and have been shown to cause hyperactivity by interfering with the autoinhibition mediated by the ID of CARD11 (16, 37). We tested whether RNF181 could inhibit signaling by six CARD11 hyperac-

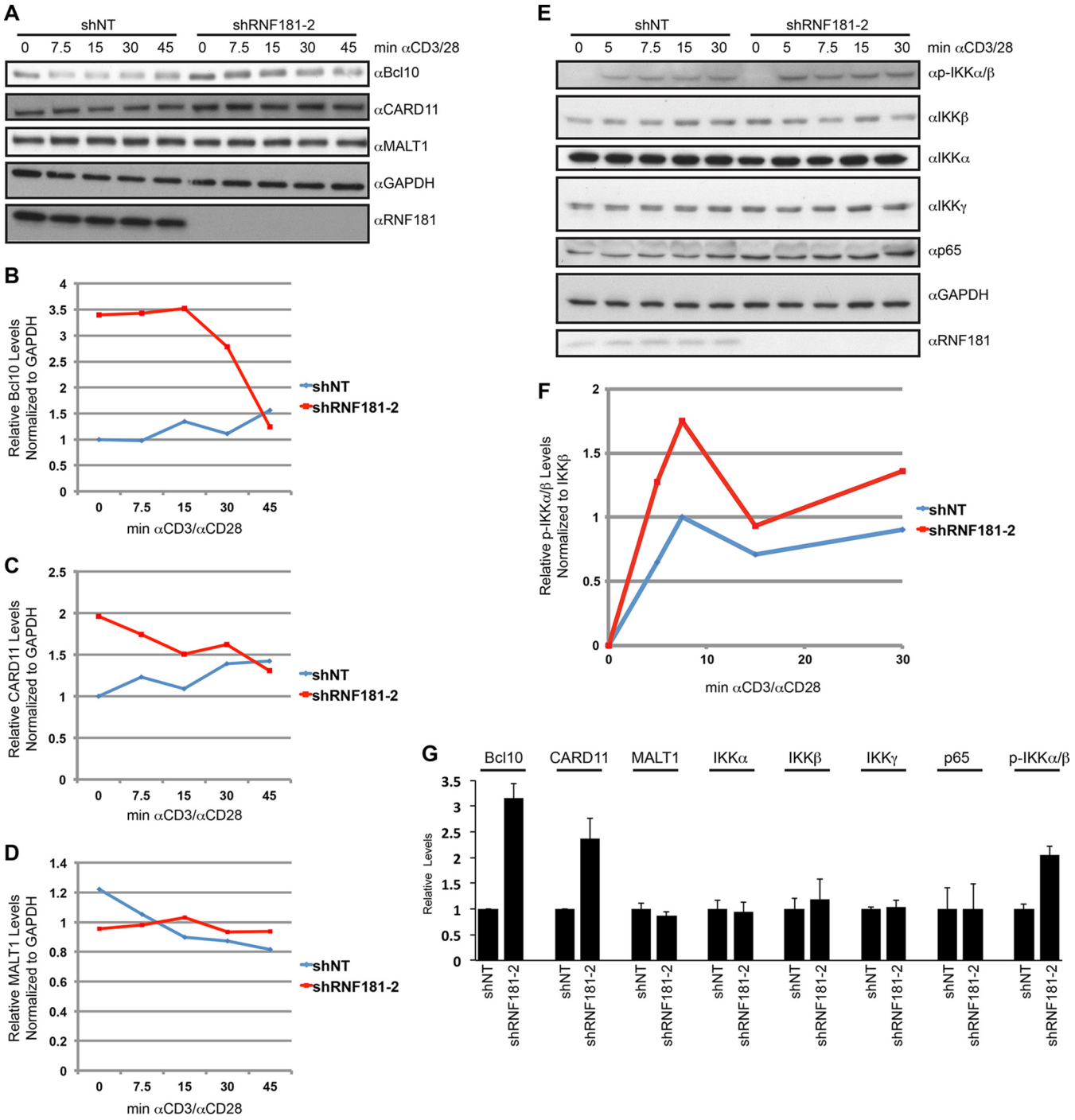

FIG 6 Bcl10 is basally upregulated in RNF181-deficient cells. (A and E) Results of representative experiments in which RNF181-deficient (shRNF181-2-expressing) or control (shNT-expressing) Jurkat T cells were stimulated with anti-CD3/anti-CD28 for the indicated times and lysates were probed for the indicated species by Western blotting. (B to D) The relative levels of the Bcl10 (B), CARD11 (C), and MALT1 (D) proteins were quantitated by normalization to the GAPDH protein level indicated in panel A. (F) Quantitation of the levels of phosphorylated IKKα/β (p-IKKα/β) normalized to the level of total IKKβ indicated in panel E. (G) The relative levels of the indicated protein species in RNF181-deficient (shRNF181-2-expressing) and control (shNT-expressing) Jurkat T cells were quantitated in three experiments and averaged. Values are normalized to those observed in shNT-expressing cells. The levels of Bcl10, CARD11, MALT1, IKKα, IKKβ, IKKγ, and p65 were normalized to the level of GAPDH at time zero of stimulation, while the levels of phosphorylated IKKα/β were normalized to the level of total IKKβ at 7.5 min of stimulation. Error bars indicate standard deviations for 3 samples. A two-tailed unpaired Student *t* test with unequal variance resulted in the following *P* values for the comparison of the values for shRNF181-2- and shNT-expressing cells: for Bcl10, $P = 0.007$; for CARD11, $P = 0.027$; for MALT1, $P = 0.19$; for IKKα, $P = 0.71$; for IKKβ, $P = 0.46$; for IKKγ, $P = 0.37$; for p65, $P = 0.93$; for phosphorylated IKKα/β, $P = 0.002$.

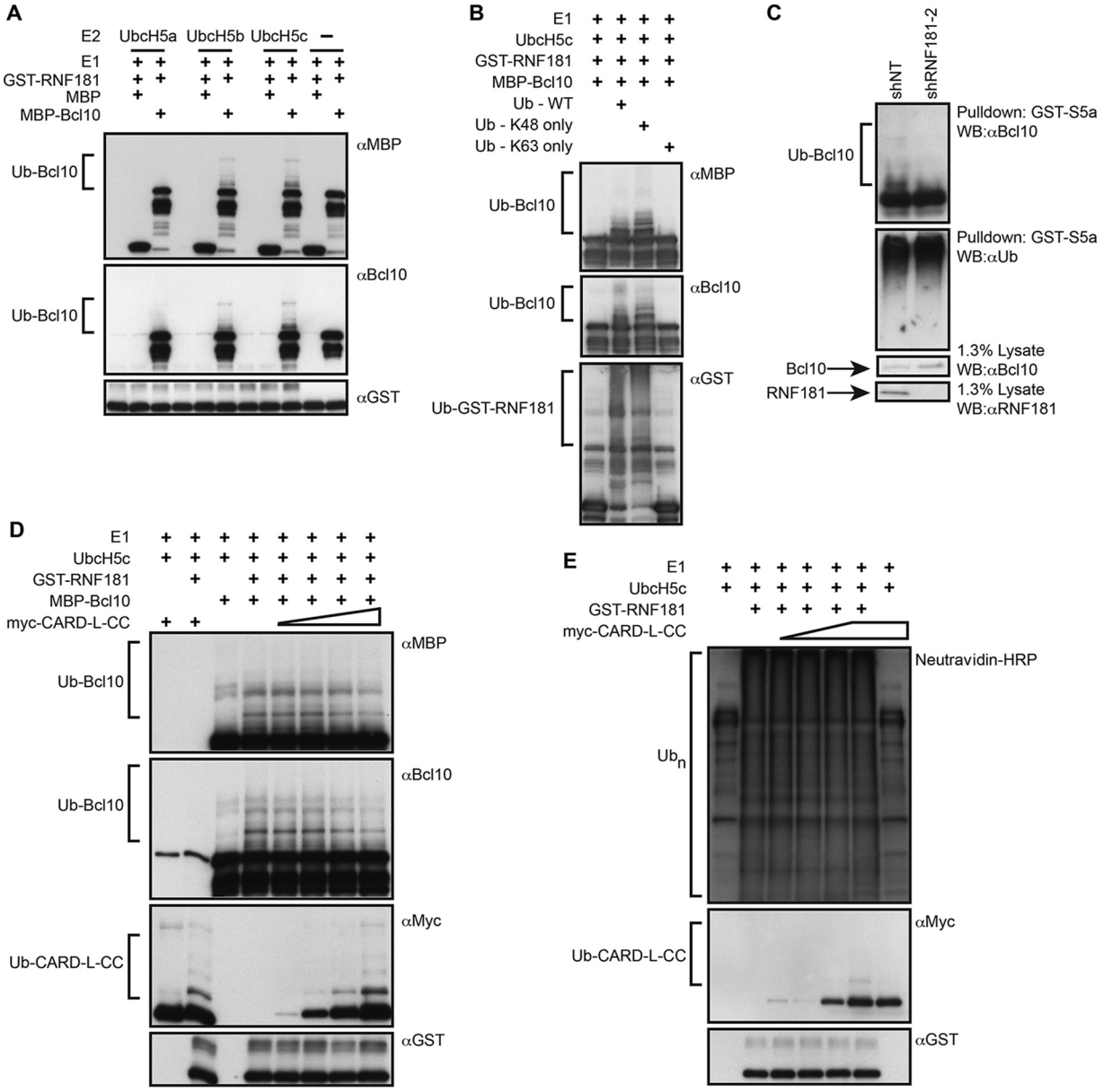

FIG 7 Bcl10 is a substrate for RNF181 E3 ubiquitin ligase activity *in vitro*. (A) Recombinant GST-RNF181 was incubated in *in vitro* ubiquitinylation reactions with E1, the indicated E2 enzymes, and either recombinant MBP-Bcl10 or MBP, as indicated. The products of the reaction were resolved on SDS-polyacrylamide gels and probed in Western blots with anti-MBP, anti-Bcl10, or anti-GST, as indicated. (B) *In vitro* ubiquitinylation reactions were performed as described in the legend to panel A with the indicated ubiquitin variants. (C) GST-S5a pulldown experiments were performed using lysates from RNF181-deficient (shRNF181-2-expressing) or control (shNT-expressing) Jurkat T cells, as described in Materials and Methods, probed with the indicated antibodies. (D and E) GST-RNF181 was incubated in *in vitro* ubiquitinylation reactions with E1, UbcH5c, recombinant MBP-Bcl10, and/or recombinant myc-CARD-L-CC, as indicated. The products of the reaction were resolved on SDS-polyacrylamide gels and probed in Western blots with the indicated antibodies.

tive variants after coexpression in HEK293T cells. Indeed, in this assay RNF181 inhibited the signaling to NF-κB by F130I, L251P, G123D, F97Y, C49Y, and V119E CARD11 variants without reducing their expression level (Fig. 8A). Interestingly, RNF181 did not associate with any of these variants in co-IP experiments (Fig. 8B) under conditions in which an association with the CARD11ΔID was apparent. This difference between the CARD11ΔID and the CARD11 gain-of-function variants is not surprising since it has previously been shown that deletion of the ID allows multiple cofactors to associate with CARD11, while the gain-of-function variants examined selectively enhance only Bcl10 association (16, 37), indicating that the gain-of-function variants only partially interfere with ID-mediated masking of the CARD and coiled-coil domains. The data are consistent with an inhibitory action of RNF181 that occurs independently of its induced association with CARD11.

To verify that endogenous concentrations of RNF181 can influence signaling by oncogenic CARD11 variants in lymphoid cells, we assayed the ability of several variants to activate the $Ig\kappa_2$-IFN-LUC reporter after transient expression in control and

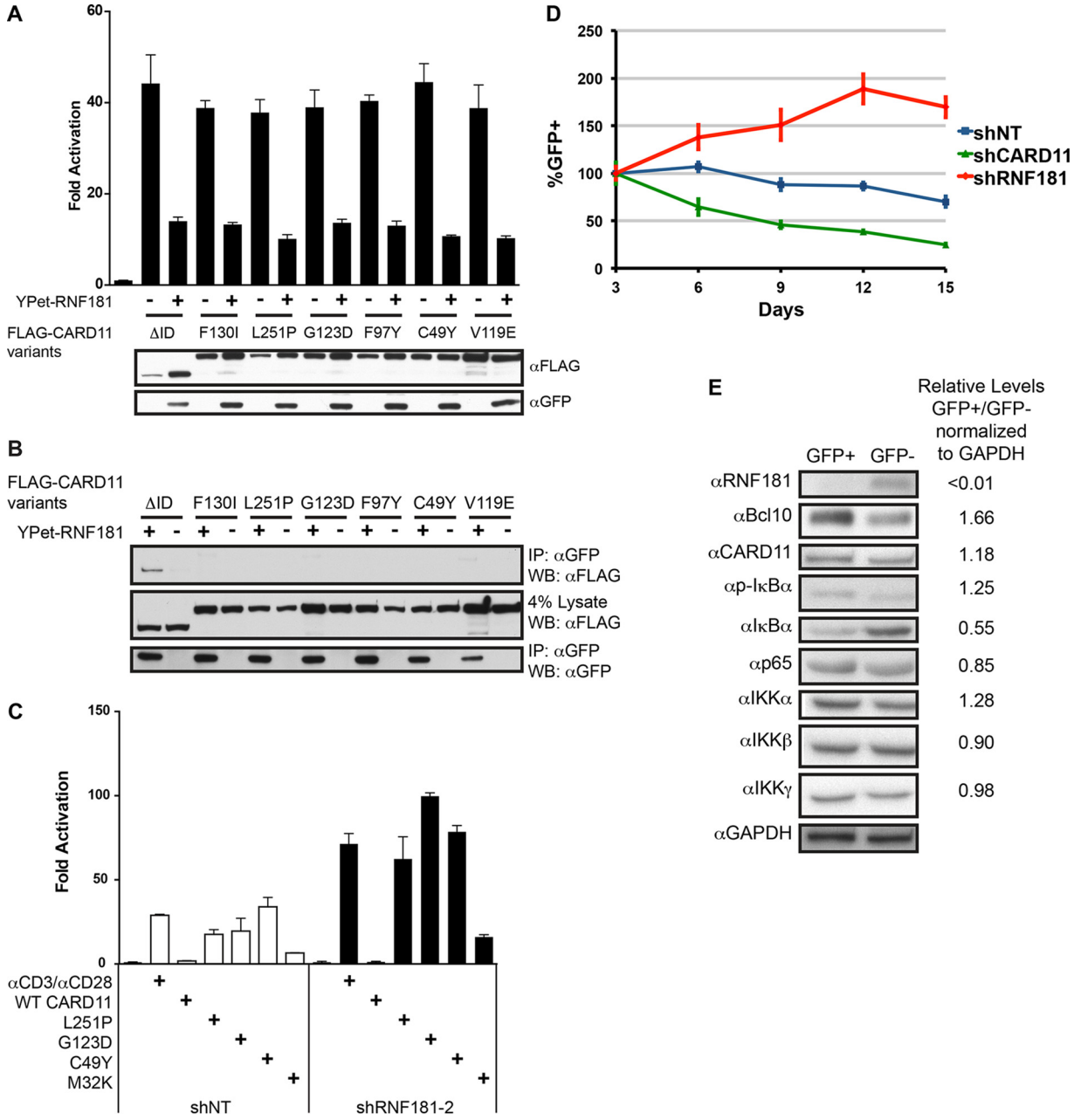

FIG 8 RNF181 inhibits signaling by oncogenic CARD11 variants and limits the proliferation of the OCI-Ly3 human ABC DLBCL cell line. (A) HEK293T cells were transfected with Igκ_2-IFN-LUC and CSK-LacZ in the absence or presence of YPet-RNF181 and the indicated FLAG-tagged CARD11 variants and assayed for fold activation of the Igκ_2-IFN-LUC reporter (top) and protein expression by Western blotting (bottom). Error bars indicate the standard deviations for 3 samples. A two-tailed unpaired Student *t* test with unequal variance resulted in *P* values of <0.009 for the comparison of each CARD11 variant in the absence and presence of YPet-RNF181. (B) HEK293T cells were transfected with expression constructs for YPet-RNF181 and the indicated FLAG-tagged CARD11 variants, and immunoprecipitations using anti-GFP antibodies were performed as described in Materials and Methods. (C) RNF181-deficient (shRNF181-2-expressing) or control (shNT-expressing) Jurkat T cells were transfected with Igκ_2-IFN-LUC and CSK-LacZ in the presence of the indicated CARD11 variants or stimulated for 4 h with anti-CD3/anti-CD28 and assayed for fold reporter activation as described in Materials and Methods. Error bars indicate the standard deviations for 3 samples. A two-tailed unpaired Student *t* test with unequal variance resulted in the following *P* values for the comparison of the values elicited by a variant in RNF181-deficient (shRNF181-2-expressing) and control (shNT-expressing) Jurkat T cells: for the wild type, $P = 0.47$; for the L251P variant, $P = 0.006$; for the G123D variant, $P = 0.00005$; for the C49Y variant, $P = 0.0002$; for the M32K variant, $P = 0.0005$. (D) OCI-Ly3 cells were infected with a retrovirus that coexpresses GFP with an shRNA that targets either CARD11 (shCARD11) or RNF181 (shRNF181-2) or a nontarget control shRNA (shNT). The percentages of GFP^+ cells were normalized to the percentages observed on day 3 after infection and were assayed until day 15. Error bars indicate the standard deviations for 3 samples. A two-tailed unpaired Student *t* test with unequal variance resulted in *P* values of <0.03 for the comparison of the normalized percentage of GFP^+ cells in cultures of either shCARD11-expressing or shRNF181-expressing cells and shNT control-expressing cells using the values obtained at days 9, 12, and 15. (E) GFP^+ and GFP^- cells from the shRNF181-expressing OCI-Ly3 culture were purified by cell sorting, and lysates were resolved on SDS-polyacrylamide gels and probed by Western blotting with the indicated antibodies. For each species, the ratio of the levels in GFP^+ cells to those in GFP^- cells normalized to the level of GAPDH is indicated.

RNF181-deficient Jurkat T cells. The absence of RNF181 in the shRNF181-2-expressing cell line resulted in enhanced NF-κB activation by the L251P, G123D, C49Y, and M32K CARD11 variants (Fig. 8C), as expected.

The OCI-Ly3 cell line, derived from a human DLBCL, harbors the oncogenic L251P allele of CARD11 that drives the constitutive activation of NF-κB that is required for proliferation and survival of the cell line in tissue culture (31). Knockdown of CARD11, Bcl10, or MALT1 in OCI-Ly3 cells leads to the decreased survival of OCI-Ly3 cells in culture (30). We adapted an assay established by Lenz et al. (31) to test whether RNF181 could modulate OCI-Ly3 proliferation. In this assay, a retrovirus expressing an shRNA linked to GFP expression is used to transduce OCI-Ly3 cells, and the fraction of GFP^+ cells in culture is monitored over time to gauge the effect of knockdown on OCI-Ly3 growth. As previously shown (16, 31), expression of an shRNA that targets the endogenous L251P CARD11 allele resulted in a reduction in the percentage of GFP^+ cells over 15 days in culture, compared to that observed with the shNT-expressing control (Fig. 8D). In contrast, expression of an shRNA that targets RNF181 resulted in enhanced OCI-Ly3 growth, which was reflected in an increase in the percentage of GFP^+ cells. We assayed GFP^+ and GFP^- cells from the OCI-Ly3 sample infected with the virus expressing the shRNA to RNF181 and found efficient knockdown of RNF181 in the GFP^+ cells compared to the control GFP^- cells, as expected (Fig. 8E). We assayed the same lysates for the levels of IκBα and phospho-IκBα and found higher levels of phospho-IκBα and lower levels of IκBα in RNF181-deficient OCI-Ly3 cells, consistent with an enhancement of signaling to NF-κB resulting from RNF181 depletion. We further assayed these lysates for several components of the CARD11 signaling pathway and found that the largest effect was on Bcl10 levels, which were clearly enhanced in RNF181-deficient OCI-Ly3 cells (Fig. 8E). The results are consistent with a role for RNF181 in inhibiting oncogenic CARD11 signaling in part by modulating the steady-state levels of Bcl10.

DISCUSSION

Our data establish RNF181 as a pathway-specific, transcription factor-specific, negative regulator of antigen receptor signaling to NF-κB that acts to limit the signaling output downstream of CARD11 scaffold activity. RNF181-deficient cells displayed enhanced TCR signaling to NF-κB but wild-type TCR signaling to NFAT and TNF-α signaling to NF-κB.

RNF181 acts to inhibit TCR signaling as an E3 ubiquitin ligase. The R118A mutant, which displayed impaired E3 ligase activity *in vitro*, failed to rescue inhibitory function in RNF181-depleted T cells. The R118A mutation does not affect the ability of the RING domain to associate with CARD11, indicating that the mutation does not impact the RING domain structure.

A plausible target for RNF181 inhibitory E3 ligase activity in this pathway is the obligate CARD11 signaling cofactor Bcl10. RNF181-deficient T cells have increased steady-state levels of Bcl10 even in the absence of antigen receptor triggering. In addition, Bcl10 can serve as a direct target for ubiquitinylation with K48-linked ubiquitin chains by RNF181 *in vitro*. Furthermore, polyubiquitinylated Bcl10 species, recognized by the proteasomal subunit S5a, can be detected in control unstimulated T cells, and lower levels are present in RNF181-deficient T cells. The results are consistent with a model in which RNF181 modulates Bcl10 levels in T cells by constitutively targeting a fraction of Bcl10 molecules for ubiquitinylation and subsequent degradation by the 26S proteasome. In this model, the levels of Bcl10 in the basal state determine the amount of CARD11-Bcl10 complexes that form upon antigen receptor triggering, which then determines the quantitative output of signaling downstream that results in NF-κB activation. It is likely that the elevated levels of Bcl10 in RNF181-deficient cells largely explain the enhanced signaling to NF-κB, since several studies have already established that the signal-induced regulation of Bcl10 levels by proteasomal, lysosomal, or autophagosomal degradation can limit the extent of TCR signaling to NF-κB (19, 23–26). These signal-dependent degradative processes target Bcl10 for destruction by other enzymes only after Bcl10 has been recruited to CARD11 and downstream signaling has ensued, and they are presumably responsible for the drop in Bcl10 levels during signaling that we observed in RNF181-depleted cells. The action of RNF181 on Bcl10, directly or indirectly, would be the first description to our knowledge of a mechanism that regulates Bcl10 levels prior to the initiation of antigen receptor signaling.

CARD11 itself may also be a relevant direct or indirect target for RNF181 E3 ligase activity. RNF181 depletion in Jurkat T cells also results in the modest elevation of CARD11 levels under basal conditions that could influence the signaling output of the pathway. CARD11 can also be ubiquitinylated by RNF181 *in vitro*. Interestingly, the addition of the recombinant CARD–LATCH–coiled-coil fragment of CARD11 to the *in vitro* ubiquitinylation reaction mixture inhibited the modification of Bcl10 by RNF181 without affecting RNF181 E3 activity *per se*. These observations suggest that the association of Bcl10 with CARD11 that is induced by signaling protects Bcl10 from RNF181 action. It is important to note that other targets of RNF181 that we have not examined may also contribute to the inhibitory effects of RNF181 on the antigen receptor signaling pathway.

Although our data clearly reveal that RNF181 and wild-type CARD11 do interact in T cells in an inducible, signal-dependent manner through the RING domain of RNF181 and the coiled-coil domain of CARD11, our evidence argues that RNF181 appears to exert its inhibitory activity prior to its signal-induced stable association with CARD11. RNF181 affects the steady-state levels of Bcl10 and, to a lesser extent, CARD11 prior to receptor triggering and, therefore, prior to its induced stable association with CARD11. Furthermore, RNF181 inhibits signaling by several oncogenic, gain-of-function CARD11 variants to which it does not stably associate, consistent with the notion that it targets its relevant substrate independently of stable binding to CARD11. Our *in vitro* E3 studies suggest that the association of RNF181 with CARD11 does not inhibit its intrinsic E3 activity. It is possible that the stable binding of RNF181 to CARD11 induced during signaling allows RNF181 to target other substrates that remain to be identified.

Our study of RNF181 in human DLBCL-derived OCI-Ly3 cells clearly suggests that RNF181 can be an important determinant of the signaling output of oncogenic CARD11 variants in the context of DLBCL. OCI-Ly3 cells proliferate in culture in a manner that is dependent on the activity of the endogenous CARD11 L251P oncogenic mutant, which drives the constitutive NF-κB activation that supports lymphoma cell survival (31). Our data indicate that the depletion of RNF181 in OCI-Ly3 cells results in a proliferative advantage, consistent with the notion that RNF181 action limits the output of oncogenic CARD11 signaling and the assumption

that the extent to which gain-of-function CARD11 mutations can support DLBCL proliferation is proportional to their quantitative ability to activate NF-κB. It is likely, therefore, that the loss of RNF181 in some lymphomas may influence oncogenic proliferation rates and perhaps allow weaker gain-of-function CARD11 alleles to support growth when they otherwise would not in the presence of wild-type RNF181. Consistent with the results observed in Jurkat T cells, the signaling component most affected by RNF181 depletion in OCI-Ly3 cells was Bcl10, supporting the hypothesis that RNF181 limits oncogenic CARD11 signaling in part by reducing the pool of Bcl10 that can interact with CARD11 and signal during dysregulated CARD11 signaling. To our knowledge, all signaling components between CARD11 and NF-κB are common to both B cells and T cells, so it is not surprising that RNF181 can modulate both normal CARD11-dependent signaling in Jurkat T cells and dysregulated CARD11-initiated signaling in OCI-Ly3 B cells. It will be important to further investigate whether and how RNF181 might affect the proliferation and survival of other ABC DLBCL samples that harbor other gain-of-function CARD11 alleles or that express wild-type CARD11 in the presence of other genetic legions that hyperactivate the NF-κB signaling pathway.

RNF181 emerged as a CARD11 interactor as a result of our development of the BRIC method. This interaction cloning strategy offers several advantages for the identification of novel biologically relevant protein-protein interactions. First, the bait-prey interaction occurs and is detected in living mammalian cells. This allows the normal cellular localization, processing, and posttranslational modification of the proteins being assayed, and the assay occurs in the same biological context in which the bait protein functions. Second, the strategy is highly modular and easily adaptable for many applications. For example, many different baits can be screened with the same YPet-fusion library, different libraries can be screened with the same bait, and multiple mammalian cell types can be used for screening. Third, BRET is easily quantitated using a luminometer with appropriate emission filters, allowing a quantitative readout of the screen. Fourth, BRET is highly dependent on the distance between the donor and the acceptor. The efficiency of energy transfer is proportional to the inverse of the sixth power of the distance between the two (45), making BRET detection in living cells a stringent indication of the proximity between bait and prey proteins. Fifth, YPet-fusion library clones can be screened in pools or individually, allowing the use of high-throughput strategies that can be tailored to a particular application. Once a positive pool is identified, sib selection can be used to break down the pool into smaller and smaller positive subpools until the individual cDNA responsible for the pool's activity is isolated and sequenced. Sixth, since the BRET interaction is detected in living cells, the screen can easily be adapted to look for signal-inducible interactions or interactions that are dependent on treatment with a pharmacological agent. For example, if one seeks proteins that interact with a bait only after cells are treated with a particular receptor ligand or drug, then a pool can be assayed for BRET in the absence and presence of the relevant agent.

ACKNOWLEDGMENTS

We thank John Bettridge, Neil Neumann, and Alyssa Ward for critical reading of the manuscript and Mollie Meffert, Steve Desiderio, and Ed Harhaj for helpful discussions and advice.

This work was supported by National Institutes of Health grants RO1CA177600 and R21AI118606 and funds from The Johns Hopkins University Institute for Cell Engineering. D.S.M. was supported by Ruth L. Kirschstein National Research Service Award F31CA171532. J.L.P. is a Leukemia and Lymphoma Society Scholar.

We declare no conflicts of interest.

FUNDING INFORMATION

HHS | NIH | National Cancer Institute (NCI) provided funding to Sarah Pedersen, Rakhi Jattani, deMauri Mackie, and Joel Pomerantz under grant number RO1CA177600. HHS | NIH | National Cancer Institute (NCI) provided funding to deMauri Mackie under grant number F31CA171532. HHS | NIH | National Institute of Allergy and Infectious Diseases (NIAID) provided funding to Sarah Pedersen, Rakhi Jattani, deMauri Mackie, and Joel Pomerantz under grant number R21AI118606.

The funders had no role in study design, data collection and interpretation, or the decision to submit the work for publication.

REFERENCES

1. **Schulze-Luehrmann J, Ghosh S.** 2006. Antigen-receptor signaling to nuclear factor kappa B. Immunity **25:**701–715. http://dx.doi.org/10.1016/j.immuni.2006.10.010.
2. **Vallabhapurapu S, Karin M.** 2009. Regulation and function of NF-κB transcription factors in the immune system. Annu Rev Immunol **27:**693–733. http://dx.doi.org/10.1146/annurev.immunol.021908.132641.
3. **Turvey SE, Durandy A, Fischer A, Fung SY, Geha RS, Gewies A, Giese T, Greil J, Keller B, McKinnon ML, Neven B, Rozmus J, Ruland J, Snow AL, Stepensky P, Warnatz K.** 2014. The CARD11-BCL10-MALT1 (CBM) signalosome complex: stepping into the limelight of human primary immunodeficiency. J Allergy Clin Immunol **134:**276–284. http://dx.doi.org/10.1016/j.jaci.2014.06.015.
4. **Perez de Diego R, Sanchez-Ramon S, Lopez-Collazo E, Martinez-Barricarte R, Cubillos-Zapata C, Ferreira Cerdan A, Casanova JL, Puel A.** 2015. Genetic errors of the human caspase recruitment domain-B-cell lymphoma 10-mucosa-associated lymphoid tissue lymphoma-translocation gene 1 (CBM) complex: molecular, immunologic, and clinical heterogeneity. J Allergy Clin Immunol **136:**1139–1149. http://dx.doi.org/10.1016/j.jaci.2015.06.031.
5. **Gaide O, Favier B, Legler DF, Bonnet D, Brissoni B, Valitutti S, Bron C, Tschopp J, Thome M.** 2002. CARMA1 is a critical lipid raft-associated regulator of TCR-induced NF-kappa B activation. Nat Immunol **3:**836–843. http://dx.doi.org/10.1038/ni830.
6. **Wang D, You Y, Case SM, McAllister-Lucas LM, Wang L, DiStefano PS, Nunez G, Bertin J, Lin X.** 2002. A requirement for CARMA1 in TCR-induced NF-kappa B activation. Nat Immunol **3:**830–835. http://dx.doi.org/10.1038/ni824.
7. **Pomerantz JL, Denny EM, Baltimore D.** 2002. CARD11 mediates factor-specific activation of NF-kappaB by the T cell receptor complex. EMBO J **21:**5184–5194. http://dx.doi.org/10.1093/emboj/cdf505.
8. **Hara H, Wada T, Bakal C, Kozieradzki I, Suzuki S, Suzuki N, Nghiem M, Griffiths EK, Krawczyk C, Bauer B, D'Acquisto F, Ghosh S, Yeh WC, Baier G, Rottapel R, Penninger JM.** 2003. The MAGUK family protein CARD11 is essential for lymphocyte activation. Immunity **18:**763–775. http://dx.doi.org/10.1016/S1074-7613(03)00148-1.
9. **Jun JE, Wilson LE, Vinuesa CG, Lesage S, Blery M, Miosge LA, Cook MC, Kucharska EM, Hara H, Penninger JM, Domashenz H, Hong NA, Glynne RJ, Nelms KA, Goodnow CC.** 2003. Identifying the MAGUK protein Carma-1 as a central regulator of humoral immune responses and atopy by genome-wide mouse mutagenesis. Immunity **18:**751–762. http://dx.doi.org/10.1016/S1074-7613(03)00141-9.
10. **Egawa T, Albrecht B, Favier B, Sunshine MJ, Mirchandani K, O'Brien W, Thome M, Littman DR.** 2003. Requirement for CARMA1 in antigen receptor-induced NF-kappa B activation and lymphocyte proliferation. Curr Biol **13:**1252–1258. http://dx.doi.org/10.1016/S0960-9822(03)00491-3.
11. **Newton K, Dixit VM.** 2003. Mice lacking the CARD of CARMA1 exhibit defective B lymphocyte development and impaired proliferation of their B and T lymphocytes. Curr Biol **13:**1247–1251. http://dx.doi.org/10.1016/S0960-9822(03)00458-5.
12. **Stepensky P, Keller B, Buchta M, Kienzler AK, Elpeleg O, Somech R, Cohen S, Shachar I, Miosge LA, Schlesier M, Fuchs I, Enders A, Eibel H, Grimbacher B, Warnatz K.** 2013. Deficiency of caspase recruitment

domain family, member 11 (CARD11), causes profound combined immunodeficiency in human subjects. J Allergy Clin Immunol **131:**477–485.e1. http://dx.doi.org/10.1016/j.jaci.2012.11.050.
13. **Greil J, Rausch T, Giese T, Bandapalli OR, Daniel V, Bekeredjian-Ding I, Stutz AM, Drees C, Roth S, Ruland J, Korbel JO, Kulozik AE.** 2013. Whole-exome sequencing links caspase recruitment domain 11 (CARD11) inactivation to severe combined immunodeficiency. J Allergy Clin Immunol **131:**1376–1383.e3. http://dx.doi.org/10.1016/j.jaci.2013.02.012.
14. **Hayden MS, Ghosh S.** 2012. NF-kappaB, the first quarter-century: remarkable progress and outstanding questions. Genes Dev **26:**203–234. http://dx.doi.org/10.1101/gad.183434.111.
15. **McCully RR, Pomerantz JL.** 2008. The protein kinase C-responsive inhibitory domain of CARD11 functions in NF-kappaB activation to regulate the association of multiple signaling cofactors that differentially depend on Bcl10 and MALT1 for association. Mol Cell Biol **28:**5668–5686. http://dx.doi.org/10.1128/MCB.00418-08.
16. **Chan W, Schaffer TB, Pomerantz JL.** 2013. A quantitative signaling screen identifies CARD11 mutations in the CARD and LATCH domains that induce Bcl10 ubiquitination and human lymphoma cell survival. Mol Cell Biol **33:**429–443. http://dx.doi.org/10.1128/MCB.00850-12.
17. **Matsumoto R, Wang D, Blonska M, Li H, Kobayashi M, Pappu B, Chen Y, Lin X.** 2005. Phosphorylation of CARMA1 plays a critical role in T cell receptor-mediated NF-kappaB activation. Immunity **23:**575–585. http://dx.doi.org/10.1016/j.immuni.2005.10.007.
18. **Sommer K, Guo B, Pomerantz JL, Bandaranayake AD, Moreno-Garcia ME, Ovechkina YL, Rawlings DJ.** 2005. Phosphorylation of the CARMA1 linker controls NF-kappaB activation. Immunity **23:**561–574. http://dx.doi.org/10.1016/j.immuni.2005.09.014.
19. **Wegener E, Oeckinghaus A, Papadopoulou N, Lavitas L, Schmidt-Supprian M, Ferch U, Mak TW, Ruland J, Heissmeyer V, Krappmann D.** 2006. Essential role for IkappaB kinase beta in remodeling Carma1-Bcl10-Malt1 complexes upon T cell activation. Mol Cell **23:**13–23. http://dx.doi.org/10.1016/j.molcel.2006.05.027.
20. **Shinohara H, Maeda S, Watarai H, Kurosaki T.** 2007. IkappaB kinase beta-induced phosphorylation of CARMA1 contributes to CARMA1 Bcl10 MALT1 complex formation in B cells. J Exp Med **204:**3285–3293. http://dx.doi.org/10.1084/jem.20070379.
21. **Thome M, Charton JE, Pelzer C, Hailfinger S.** 2010. Antigen receptor signaling to NF-{kappa}B via CARMA1, BCL10, and MALT1. Cold Spring Harb Perspect Biol **2:**a003004. http://dx.doi.org/10.1101/cshperspect.a003004.
22. **Paul S, Schaefer BC.** 2013. A new look at T cell receptor signaling to nuclear factor-kappaB. Trends Immunol **34:**269–281. http://dx.doi.org/10.1016/j.it.2013.02.002.
23. **Lobry C, Lopez T, Israel A, Weil R.** 2007. Negative feedback loop in T cell activation through IkappaB kinase-induced phosphorylation and degradation of Bcl10. Proc Natl Acad Sci U S A **104:**908–913. http://dx.doi.org/10.1073/pnas.0606982104.
24. **Paul S, Kashyap AK, Jia W, He YW, Schaefer BC.** 2012. Selective autophagy of the adaptor protein Bcl10 modulates T cell receptor activation of NF-kappaB. Immunity **36:**947–958. http://dx.doi.org/10.1016/j.immuni.2012.04.008.
25. **Scharschmidt E, Wegener E, Heissmeyer V, Rao A, Krappmann D.** 2004. Degradation of Bcl10 induced by T-cell activation negatively regulates NF-kappa B signaling. Mol Cell Biol **24:**3860–3873. http://dx.doi.org/10.1128/MCB.24.9.3860-3873.2004.
26. **Zeng H, Di L, Fu G, Chen Y, Gao X, Xu L, Lin X, Wen R.** 2007. Phosphorylation of Bcl10 negatively regulates T-cell receptor-mediated NF-kappaB activation. Mol Cell Biol **27:**5235–5245. http://dx.doi.org/10.1128/MCB.01645-06.
27. **Moreno-Garcia ME, Sommer K, Shinohara H, Bandaranayake AD, Kurosaki T, Rawlings DJ.** 2010. MAGUK-controlled ubiquitination of CARMA1 modulates lymphocyte NF-kappaB activity. Mol Cell Biol **30:**922–934. http://dx.doi.org/10.1128/MCB.01129-09.
28. **Lamason RL, Kupfer A, Pomerantz JL.** 2010. The dynamic distribution of CARD11 at the immunological synapse is regulated by the inhibitor kinesin GAKIN. Mol Cell **40:**798–809. http://dx.doi.org/10.1016/j.molcel.2010.11.007.
29. **Davis RE, Brown KD, Siebenlist U, Staudt LM.** 2001. Constitutive nuclear factor kappaB activity is required for survival of activated B cell-like diffuse large B cell lymphoma cells. J Exp Med **194:**1861–1874. http://dx.doi.org/10.1084/jem.194.12.1861.
30. **Ngo VN, Davis RE, Lamy L, Yu X, Zhao H, Lenz G, Lam LT, Dave S, Yang L, Powell J, Staudt LM.** 2006. A loss-of-function RNA interference screen for molecular targets in cancer. Nature **441:**106–110. http://dx.doi.org/10.1038/nature04687.
31. **Lenz G, Davis RE, Ngo VN, Lam L, George TC, Wright GW, Dave SS, Zhao H, Xu W, Rosenwald A, Ott G, Muller-Hermelink HK, Gascoyne RD, Connors JM, Rimsza LM, Campo E, Jaffe ES, Delabie J, Smeland EB, Fisher RI, Chan WC, Staudt LM.** 2008. Oncogenic CARD11 mutations in human diffuse large B cell lymphoma. Science **319:**1676–1679. http://dx.doi.org/10.1126/science.1153629.
32. **Compagno M, Lim WK, Grunn A, Nandula SV, Brahmachary M, Shen Q, Bertoni F, Ponzoni M, Scandurra M, Califano A, Bhagat G, Chadburn A, Dalla-Favera R, Pasqualucci L.** 2009. Mutations of multiple genes cause deregulation of NF-kappaB in diffuse large B-cell lymphoma. Nature **459:**717–721. http://dx.doi.org/10.1038/nature07968.
33. **Lohr JG, Stojanov P, Lawrence MS, Auclair D, Chapuy B, Sougnez C, Cruz-Gordillo P, Knoechel B, Asmann YW, Slager SL, Novak AJ, Dogan A, Ansell SM, Link BK, Zou L, Gould J, Saksena G, Stransky N, Rangel-Escareno C, Fernandez-Lopez JC, Hidalgo-Miranda A, Melendez-Zajgla J, Hernandez-Lemus E, Schwarz-Cruz y Celis A, Imaz-Rosshandler I, Ojesina AI, Jung J, Pedamallu CS, Lander ES, Habermann TM, Cerhan JR, Shipp MA, Getz G, Golub TR.** 2012. Discovery and prioritization of somatic mutations in diffuse large B-cell lymphoma (DLBCL) by whole-exome sequencing. Proc Natl Acad Sci U S A **109:**3879–3884. http://dx.doi.org/10.1073/pnas.1121343109.
34. **Montesinos-Rongen M, Schmitz R, Brunn A, Gesk S, Richter J, Hong K, Wiestler OD, Siebert R, Kuppers R, Deckert M.** 2010. Mutations of CARD11 but not TNFAIP3 may activate the NF-kappaB pathway in primary CNS lymphoma. Acta Neuropathol **120:**529–535. http://dx.doi.org/10.1007/s00401-010-0709-7.
35. **Bu R, Bavi P, Abubaker J, Jehan Z, Al-Haqawi W, Ajarim D, Al-Dayel F, Uddin S, Al-Kuraya KS.** 2012. Role of NF-kappaB regulators-TNFAIP3 and CARD11 in Middle Eastern diffuse large B cell lymphoma. Leuk Lymphoma **53:**1971–1977. http://dx.doi.org/10.3109/10428194.2012.668286.
36. **Dong G, Chanudet E, Zeng N, Appert A, Chen YW, Au WY, Hamoudi RA, Watkins AJ, Ye H, Liu H, Gao Z, Chuang SS, Srivastava G, Du MQ.** 2011. A20, ABIN-1/2, and CARD11 mutations and their prognostic value in gastrointestinal diffuse large B-cell lymphoma. Clin Cancer Res **17:**1440–1451. http://dx.doi.org/10.1158/1078-0432.CCR-10-1859.
37. **Lamason RL, McCully RR, Lew SM, Pomerantz JL.** 2010. Oncogenic CARD11 mutations induce hyperactive signaling by disrupting autoinhibition by the PKC-responsive inhibitory domain. Biochemistry **49:**8240–8250. http://dx.doi.org/10.1021/bi101052d.
38. **Makowski SL, Wang Z, Pomerantz JL.** 2015. A protease-independent function for SPPL3 in NFAT activation. Mol Cell Biol **35:**451–467. http://dx.doi.org/10.1128/MCB.01124-14.
39. **Hamdan FF, Percherancier Y, Breton B, Bouvier M.** 2006. Monitoring protein-protein interactions in living cells by bioluminescence resonance energy transfer (BRET). Curr Protoc Neurosci **Chapter 5:**Unit 5.23. http://dx.doi.org/10.1002/0471142301.ns0523s34.
40. **Loening AM, Fenn TD, Wu AM, Gambhir SS.** 2006. Consensus guided mutagenesis of Renilla luciferase yields enhanced stability and light output. Protein Eng Des Sel **19:**391–400. http://dx.doi.org/10.1093/protein/gzl023.
41. **Nguyen AW, Daugherty PS.** 2005. Evolutionary optimization of fluorescent proteins for intracellular FRET. Nat Biotechnol **23:**355–360. http://dx.doi.org/10.1038/nbt1066.
42. **Plechanovova A, Jaffray EG, McMahon SA, Johnson KA, Navratilova I, Naismith JH, Hay RT.** 2011. Mechanism of ubiquitylation by dimeric RING ligase RNF4. Nat Struct Mol Biol **18:**1052–1059. http://dx.doi.org/10.1038/nsmb.2108.
43. **Plechanovova A, Jaffray EG, Tatham MH, Naismith JH, Hay RT.** 2012. Structure of a RING E3 ligase and ubiquitin-loaded E2 primed for catalysis. Nature **489:**115–120. http://dx.doi.org/10.1038/nature11376.
44. **Zhang N, Wang Q, Ehlinger A, Randles L, Lary JW, Kang Y, Haririnia A, Storaska AJ, Cole JL, Fushman D, Walters KJ.** 2009. Structure of the S5a:K48-linked diubiquitin complex and its interactions with rpn13. Mol Cell **35:**280–290. http://dx.doi.org/10.1016/j.molcel.2009.06.010.
45. **Eidne KA, Kroeger KM, Hanyaloglu AC.** 2002. Applications of novel resonance energy transfer techniques to study dynamic hormone receptor interactions in living cells. Trends Endocrinol Metab **13:**415–421. http://dx.doi.org/10.1016/S1043-2760(02)00669-0.